iScience

CellPress

Article

Tissue-Specific Chk1 Activation Determines Apoptosis by Regulating the Balance of p53 and p21

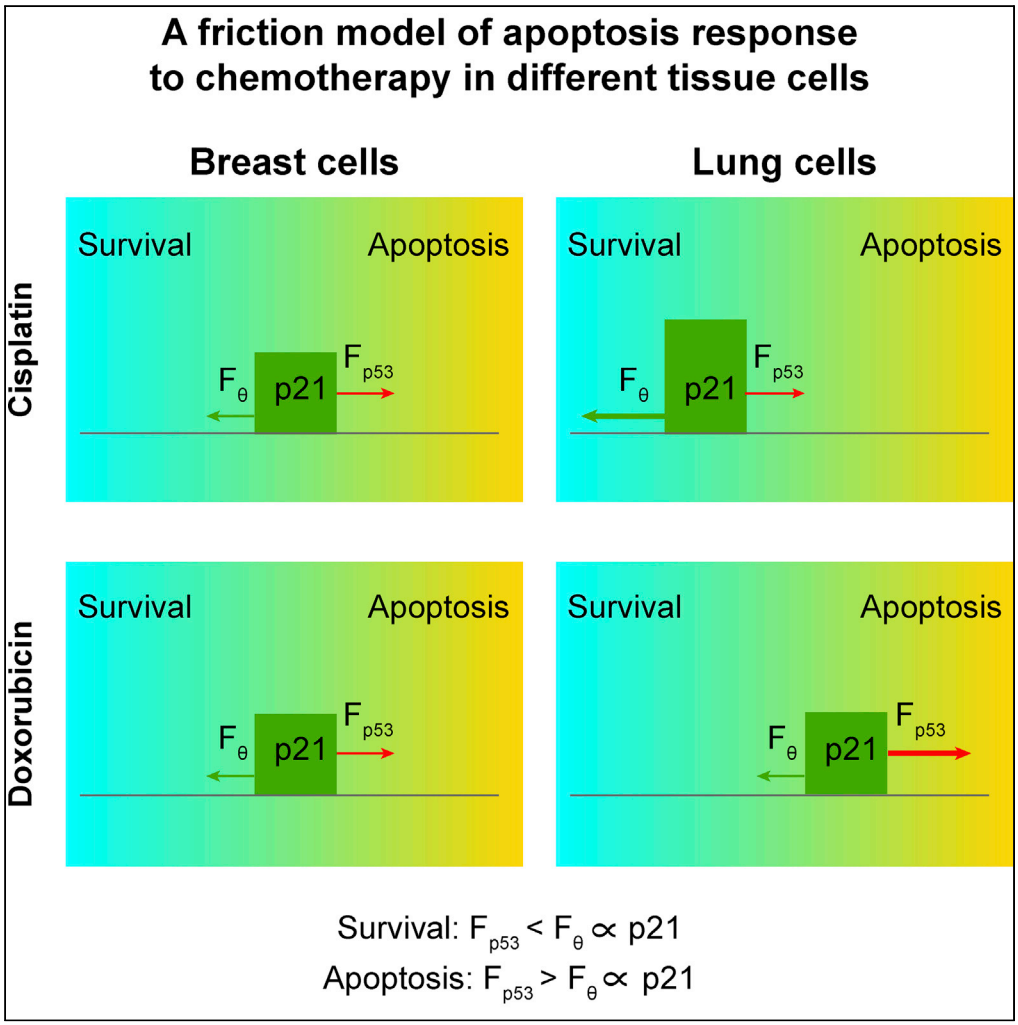

Marijn T.M. van Jaarsveld, Difan Deng, Erik A.C. Wiemer, Zhike Zi

zhike.zi@molgen.mpg.de

HIGHLIGHTS

Breast and lung cells show different sensitivities to chemotherapeutic drugs

Lung cells activate Chk1 more strongly than breast cells with chemotherapeutic drugs

Active Chk1 plays a regulatory role in p53 activation and apoptosis responses

The balance of p53 and p21 dynamics drives the apoptosis response to DNA damage

van Jaarsveld et al., iScience *12*, 27–40
February 22, 2019
https://doi.org/10.1016/j.isci.2019.01.001

iScience

CellPress

Article

Tissue-Specific Chk1 Activation Determines Apoptosis by Regulating the Balance of p53 and p21

Marijn T.M. van Jaarsveld,[1] Difan Deng,[1] Erik A.C. Wiemer,[2] and Zhike Zi[1,3,*]

SUMMARY

The DNA damage response (DDR) protects cells against genomic instability. Surprisingly, little is known about the differences in DDR across tissues, which may affect cancer evolutionary trajectories and chemotherapy response. Using mathematical modeling and quantitative experiments, we found that the DDR is regulated differently in human breast and lung primary cells. Equal levels of cisplatin-DNA lesions caused stronger Chk1 activation in lung cells, leading to resistance. In contrast, breast cells were more resistant and showed more Chk2 activation in response to doxorubicin. Further analyses indicate that Chk1 activity played a regulatory role in p53 phosphorylation, whereas Chk2 activity was essential for p53 activation and p21 expression. We propose a novel "friction model," in which the balance of p53 and p21 levels contributes to the apoptotic response in different tissues. Our results suggest that modulating the balance of p53 and p21 dynamics could optimize the response to chemotherapy.

INTRODUCTION

The DNA damage response (DDR) is an intricate signaling network that governs genomic integrity and protects against carcinogenesis. The core DDR network is formed by ATR and Chk1, ATM and Chk2, p53, and p21. ATR/Chk1 signaling is activated mostly by stresses involving single-strand DNA damage, whereas ATM and Chk2 are activated in response to double-strand breaks (DSBs) (Reinhardt and Schumacher, 2012; Smith et al., 2010; Weber and Ryan, 2015). Both ATR/Chk1 and ATM/Chk2 can activate p53, a master regulator of the DDR, which regulates cellular responses such as cell cycle arrests, repair and survival, or cell death. An important determinant of outcome is the p53 target protein p21, which can inhibit cell cycle progression and negatively regulate p53-mediated apoptosis (Abbas and Dutta, 2009).

Proper regulation of the DDR is important, because dysregulation is associated with aging and cancer (Hoeijmakers, 2009). Tumors frequently contain mutations in DDR genes and are characterized by an aberrant response to DNA damage. Strikingly, cancers originating in distinct tissues have diverse mutational signatures (Alexandrov et al., 2013; Kandoth et al., 2013; Zehir et al., 2017), suggesting that they have different DNA repair defects (Chae et al., 2016; Forestier et al., 2012; Garner and Eastman, 2011). Differences in DDR are also thought to result in specific sensitivities for DNA-damaging chemotherapy (Chae et al., 2016; Forestier et al., 2012; Liu et al., 2017; Sousa et al., 2015; Stewart-Ornstein and Lahav, 2017), which differ per cancer type. For instance, non-small-cell lung cancer responds relatively well to the DNA adduct and strand cross-linking agent cisplatin (Eastman, 1987; Gettinger and Lynch, 2011; Non-small Cell Lung Cancer Collaborative Group, 1995; Laskin and Sandler, 2005; Paoletti et al., 2011; Rosenberg et al., 1969). In contrast, the DNA-DSB-inducing drug doxorubicin is more effective in treating breast cancer (Arcamone et al., 1969; Crown, 1998; von Minckwitz, 2007).

It is unclear whether the differences in DDR in cancer types arise during tumor evolution, or whether they reflect variations present in the original tissue. It is conceivable that healthy cells have differences in the DDR network. For instance, skin cells exposed to sunlight might express a higher amount of genes involved in the repair of UV-induced DNA lesions than other tissues. In addition, mutations in DDR genes affect cancer development across tissues differently. For example, germline mutations in BRCA1/2 and Chk2 enhance cancer risk in specific tissues such as breast, whereas the added risk for tumors occurring in other tissues like lung is small (Levy-Lahad and Friedman, 2007; Michailidou et al., 2017; Nevanlinna and Bartek, 2006). Furthermore, the response to DNA damage is different across stem cell types. In particular intestinal stem cells are prone to induce apoptosis after DNA damage, whereas DNA damage in melanocytes results

[1]Max Planck Institute for Molecular Genetics, Otto Warburg Laboratory, Ihnestr. 63-73, 14195 Berlin, Germany

[2]Erasmus University Medical Center, Erasmus MC Cancer Institute, Department of Medical Oncology, Wytemaweg 80, 3015 CN Rotterdam, The Netherlands

[3]Lead Contact

*Correspondence: zhike.zi@molgen.mpg.de

https://doi.org/10.1016/j.isci.2019.01.001

in terminal differentiation (Blanpain et al., 2011; Vitale et al., 2017). A systematic comparison of the DDR across tissues is lacking. Understanding what differences in DDR network arise during tumor evolution and which ones are already present will provide more insight into tissue-specific cancer risk. In addition, this knowledge could lead to more effective targeting of tumor cells for therapy.

To address how the DDR is regulated across tissues, we used non-immortalized primary epithelial cells from multiple breast and lung donors. We focused on breast and lung cells for three reasons: (1) breast and lung tissues frequently give rise to tumors; (2) certain DDR gene mutations predispose for breast cancer, but not for lung cancer; and (3) breast and lung tumors have different sensitivities for genotoxic chemotherapy. By combining modeling and experimental approaches, we show that these cell types have different apoptotic sensitivities for genotoxic chemotherapy. We demonstrate that the difference in sensitivity originates at the earliest level of DNA damage detection: in the tissue-specific regulation of the ATR-Chk1 and ATM-Chk2 network. Our modeling and experimental analyses suggest that differential activation of Chk1 and Chk2 regulates the balance of p53 and p21 dynamics and contributes to chemotherapy responses to DNA damage in breast and lung cells. This study sheds light on the tissue-specific DDR and provides clues on how to optimize chemotherapy response.

RESULTS

An Equal Amount of Cisplatin-DNA Lesions Induces More Apoptosis in Primary Breast Than Lung Cells

The DDR pathway is a complex signaling network, which is activated upon many forms of damage and gives rise to multiple different outputs. We have focused on one DNA-damaging agent and one cellular outcome (apoptosis). To study the differences of the DDR in different cell types, we used primary breast and lung cells. We started with the platinum-containing drug cisplatin because it is a widely used chemotherapeutic that causes DNA adducts and inter- and intrastrand cross-links and is known to induce apoptosis (Eastman, 1987; Hu et al., 2016; Rosenberg et al., 1969), which can be readily quantified using MTT (*3-(4,5-Dimethylthiazol-2-yl)-2,5-diphenyltetrazolium bromide*) cell viability assay. Briefly, cells were seeded at 50% density, followed by 48 h of cisplatin exposure. This setup allowed us to measure cell death (Figure 1A). Breast cells (IC_{50}~ 15–20 μM) were consistently more sensitive than lung cells (IC_{50}~40 μM; $p = 1 \times 10^{-9}$; Figure 1B). A different sensitivity for apoptosis was confirmed by the appearance of apoptotic morphology as visualized by DAPI staining (Figures 1C and 1D).

To control for differential cisplatin uptake, we looked directly at the relation between platinum bound to the DNA (Pt_DNA) and cellular outcome. Breast cells contained higher levels of Pt_DNA at similar cisplatin doses (Figure S1A), and even when corrected for the amount of Pt_DNA, breast cells were consistently more sensitive for cisplatin (Figure 1E). In summary, breast cells induce apoptosis at a lower amount of DNA damage than lung cells.

Cisplatin Treatment Activates Chk1 Signaling More Strongly in Lung Cells, Resulting in Increased Resistance

To understand how an equal dose of DNA damage results in differential cell viability, we initially focused on p53 dynamics, as it is an important determinant of apoptosis. Intriguingly, p53 levels alone could not explain the differential apoptotic sensitivity. When breast and lung cells were treated with 20 and 30 μM cisplatin, DNA-bound cisplatin and total p53 levels were very similar (Figures S1B and S1C). To understand the mechanism behind their differential cisplatin sensitivity, we used protein microarrays to assess temporal changes of the proteome and phosphoproteome (covering 366 unique UniProt IDs) in breast and lung cells. We analyzed the proteome at three time points: an early stage (6 h; p53 increase becomes apparent), an intermediate stage (12 h), and a late stage (24 h), in which signs of apoptosis can be observed. We thus generated an unbiased profile of the post-DNA damage proteome in healthy breast and lung cells. Among the proteins that were differentially expressed, 17 BioCarta pathways were significantly enriched ($p < 0.1$; Figures 2A, 2B, and S2; Tables S1, S2, and S3). After antibody validation (Table S2), we focused on five differentially regulated signaling modules: PTEN/Akt signaling, ERK, p38, JNK signaling, and DNA damage checkpoint activation. As shown in Figures 2C and S3, differential activation (as measured by phosphorylation on key residues) was observed for proteins in the mitogen-activated protein kinase (MAPK) signaling pathway. For example, p38 MAPK was activated to a higher degree in primary breast cells. Furthermore, differences in DNA damage checkpoint activity were observed (Figures 2C and S3E). Active ATR (p-S428) was present at higher levels in lung cells than breast cells. Accordingly, its downstream target Chk1 was activated (S345) to a greater extent in lung cells.

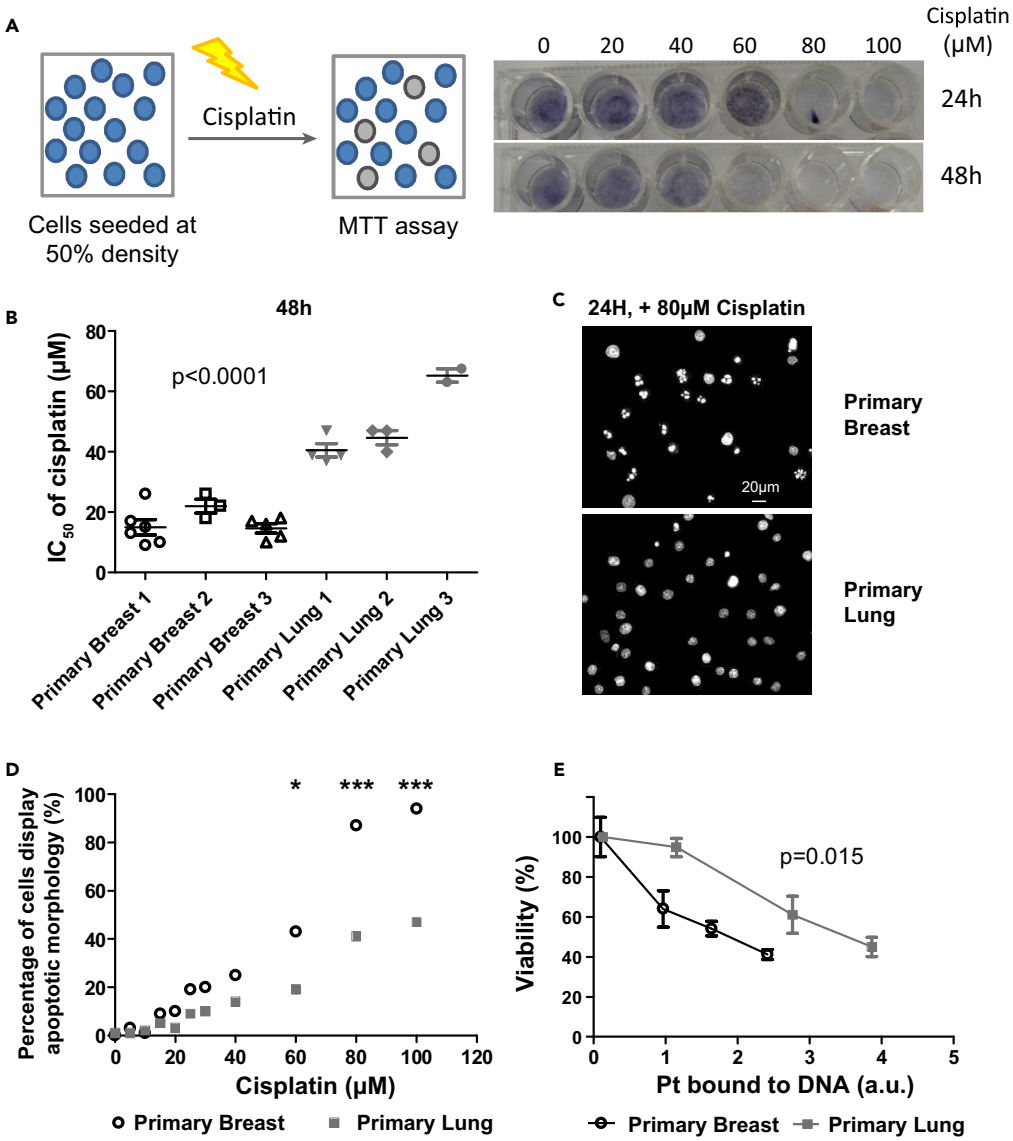

Figure 1. Primary Breast Cells Are More Sensitive to Cisplatin-Induced DNA Lesions Than Primary Lung Cells

(A) Overview of adapted MTT assay to measure cell death. Briefly, cells were seeded at 50% density and treated with high doses of cisplatin for 24 or 48 h. Treatment under these conditions results in cell death (e.g., compare the wells treated with 60 μM cisplatin at 24 and 48 h).

(B) Breast cells are more sensitive to cisplatin than lung cells. Human primary epithelial cells from six donors were treated with a range of cisplatin concentrations. After 48 h, the cell viability was determined by MTT assay. The concentration at which 50% loss of viability occurred (IC_{50}) was calculated (n = 3–6). A *t*-test was used to compare IC_{50} values between breast and lung cells.

(C) Treatment with cisplatin results in apoptosis. Nuclear morphology of breast and lung cells was visualized by DAPI stain after 24-h exposure to 80 μM cisplatin (representative experiment, n = 4).

(D) Breast cells more frequently display apoptotic morphology (DAPI stain) after 24 h of cisplatin treatment than lung cells (representative experiment, n = 4). A two-way ANOVA with Bonferroni post-hoc test was carried out to compare differences (*$p < 0.05$, ***$p < 0.001$).

(E) Breast cells are more sensitive to equal amounts of cisplatin-induced DNA lesions at 48 h. The amount of DNA-bound platinum was determined after 48 h of cisplatin treatment (Figure S1A) and plotted against the cellular viability (MTT assay) at 48 h (representative experiment, n = 3). Regression analysis was used to test if the slope and intercept were different. Error bars represent the SD (n = 3).

A

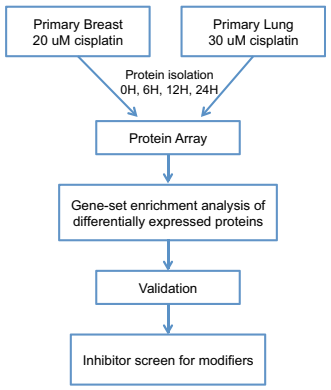

B

Biocarta pathways	%	P-value	Core modules
IL 2 signaling	7.8	0.02	JAK-STAT, RAS-MEK-ERK pathways
Ras Signaling	6.2	0.02	Ras-MEK-ERK, PI3K-Akt/PKB pathways
Phosphoinositides and downstream	6.2	0.02	PI-activated molecules
MAPKinase Signaling	20.2	0.03	Ras-MEK-ERK, p38 MAPK, JNK pathways
TPO Signaling	7.0	0.04	JAK-STAT, RAS-MEK-ERK pathways
IL 6 signaling	6.2	0.04	JAK-STAT, RAS-MEK-ERK pathways
PDGF Signaling P	8.5	0.04	JAK-STAT, RAS-MEK-ERK pathways
IL22 Soluble Receptor Signaling	3.9	0.05	JAK-STAT pathway
CBL mediated downregulation of EGF receptors	4.7	0.05	CBL and Cell surface receptors
Inhibition of Cellular Proliferation by Gleevec	7.0	0.06	JAK-STAT, RAS-MEK-ERK pathways, Akt
Ras and Rho proteins and G1 to S Transition	8.5	0.07	PI3K-Akt, Rb-Cyclin D-Cyclin E pathways
EGF Signaling	8.5	0.07	JAK-STAT, RAS-MEK-ERK pathways
Cell Cycle: G2/M Checkpoint	6.2	0.07	ATM-ATR pathway
Cytomegalovirus and Map Kinase	6.2	0.07	Akt, Ras-MAPK, p38 pathway
T Cell Receptor Signaling	9.3	0.08	RAS-MEK-ERK pathway
Sprouty regulation of tyrosine kinase signals	4.7	0.09	RAS-MEK-ERK pathway, CBL-EGFR
IL 3 signaling	4.7	0.09	JAK-STAT, RAS-MEK-ERK pathways

C

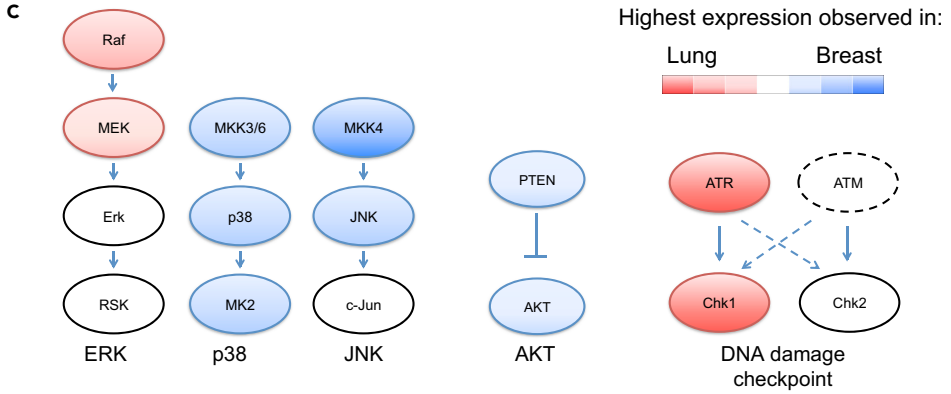

D

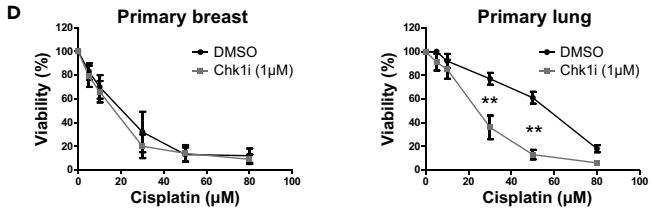

Figure 2. Proteomic and Functional Analysis Reveals an Increased Chk1 Activity in Lung Cells that Contributes to Cisplatin Resistance

(A) Identification of genes involved in differential cisplatin response. Breast and lung cells were treated with a cisplatin dose that caused an equal amount of DNA damage (20 μM and 30 μM, respectively). A protein array (366 unique UniProt IDs covered by both pan-specific and phospho-specific antibodies) was carried out to assess proteomic changes at 6, 12, and 24 h. Gene set enrichment was performed on differentially expressed proteins to identify differentially regulated pathways. After validation of the array results using both antibodies present on the array and antibodies from different manufacturers, inhibitors were used to screen for genes that modified the cisplatin response. For details see Transparent Methods and Figure S2.

(B) Overview of BioCarta pathways enriched for differentially expressed genes (DAVID pathway analysis). For details, see Table S2.

(C) Overview of the most differentially activated pathways after cisplatin treatment. After array antibody validation (Table S2), activity of differentially regulated pathways was determined using quantitative western blot (Figure S3). The colors indicate whether protein activity (e.g., highest phosphorylation levels) is the highest in lung (red) or breast (blue) cells.

(D) Inhibition of Chk1 activity differentially affects cisplatin sensitivity. Cells were treated for 1 h with the Chk1 inhibitor PF477736 (1 μM) or an equivalent amount of DMSO, after which cisplatin was added. Viability was determined after 48 h. Error bars represent the SD (n = 7). A two-way ANOVA with Bonferroni post-hoc test was carried out to test if differences were significant (**$p < 0.01$).

To investigate if the differentially regulated pathways affect cisplatin-induced apoptosis, we negatively regulated essential proteins in each pathway using specific inhibitors that produce fewer side effects than small interfering RNAs. Inhibitors for phosphatidylinositol 3-kinase, JNK, p38 kinase, and MEK did

not significantly alter the cisplatin response (Figure S4). We next focused on ATR, Chk1, and Chk2 using specific inhibitors (VE822 for ATR, PF477736 for Chk1, Chk2 inhibitor II for Chk2) (Figure S5A). Strikingly, Chk1 inhibition sensitized primary lung cells to cisplatin ($p < 0.001$), but it had no effect on breast cells (Figure 2D). Similar effects of Chk1 inhibition were observed in primary cells obtained from different donors (Table S4), and ATR inhibition sensitized lung cells too (Figures S5B and S5C). We also found that cell viability responses in lung cells were affected to a lesser extent by Chk2 inhibition than by Chk1 inhibition (Figure S5D). Taken together, these results indicate that the higher activity of Chk1 in lung cells contributes to cisplatin resistance of lung cells.

Cell-Type-Specific DNA Damage Signaling Dynamics after Cisplatin Treatment

The identification of Chk1 as a modifier of the apoptotic sensitivity for cisplatin was unexpected because its downstream target p53 accumulates to similar levels in breast and lung cells (Figure S1C). We therefore decided to compare the activity of the Chk1-Chk2-p53 signaling network in breast and lung cells more closely. We quantitatively measured the total levels and activities of Chk1, Chk2, p53, and p21 (Figure 3A). After an equal amount of cisplatin-induced DNA damage, Chk1 activity, as measured by phosphorylation of sites S345, S317, and S296, increased to a much higher level in the lung cells (Figure 3A, $p < 0.01$, Figure S6). In contrast, Chk2 activation (T68, S516) was only moderately increased in both cell types. Although total p53 levels were similar in breast and lung cells, p53 was phosphorylated (S15/S20) to a larger extent in lung cells (Figure 3A, $p < 0.01$, Figure S6), correlating with higher Chk1 activation. In addition, p21 levels increased in lung cells but not in breast cells. Together, these results show that primary breast and lung cells display different dynamics of Chk1 activation, p53 phosphorylation, and p21 protein expression after cisplatin treatment.

A Quantitative Model Predicts Differential Roles of Chk1 and Chk2 in the Regulation of p53 Phosphorylation

To better understand the relation between the dynamics of the DDR proteins and the chemotherapy response (apoptosis), we developed an integrated mathematical model based on our current data and previous studies (Barr et al., 2017; Batchelor et al., 2008, 2011; Ma et al., 2005; Stewart-Ornstein and Lahav, 2017; Zhang et al., 2011). This new model consists of coupled ordinary differential equations, and it focuses on the key interactions between Chk1, Chk2, p53, and p21 (Figure S7). In the model, we used the same model structure and reaction kinetics for breast and lung cells. Most parameters have the same values, except that some parameters are set with cell-type-specific values to distinguish different cisplatin-DNA binding dynamics, differential activation, and degradation of proteins observed in breast and lung cells (list of parameter values is given in Tables S5–S7). A detailed description of the model development, model simulation, and parameter estimation is provided in the Supplemental Information.

The mathematical model was fitted to the experimental datasets that captured the temporal profiles of cisplatin-DNA binding dynamics; total levels of Chk1, Chk2, p53, and p21; the activation of Chk1, Chk2, and p53; as well as cell viability responses in breast and lung cells. In total, 98 average values (from 564 measured data points) were used to estimate the kinetic parameters of the model for cisplatin treatment. As shown in Figures 3B and S8, the model simulations quantitatively fit the signaling dynamics of Chk1, Chk2, p53, and p21 proteins and DNA-bound cisplatin.

Intriguingly, the model suggested that the contribution of Chk1 and Chk2 to the regulation of p53 and p21 dynamics is different. As shown in Figure S9, the modeling analyses indicate that Chk2 activities in breast and lung cells are relatively high and give rise to a saturated p53 phosphorylation rate. On the other hand, in breast cells Chk1 activity is too low to induce p53 phosphorylation, whereas its level in lung cells is relatively high and induces additional p53 phosphorylation on top of Chk2's activity. We next studied what happens to downstream p53 and p21 responses after *in silico* inhibition of Chk1 and Chk2 activities (details are in Supplemental Information). The model predicted that Chk1 inhibition has almost no effect on p53 and p21 dynamics in breast cells, where Chk1 phosphorylation is low (Figure 4A). In contrast, in lung cells a strong effect of Chk1 inhibition on p53 and p21 dynamics is expected (Figure 4B). Interestingly, it is also predicted that Chk2 inhibition will strongly decrease the levels of total p53, p53 phosphorylation, and p21 in both breast and lung cells (Figures 4A and 4B). These results thus indicate that the contributions of Chk1 and Chk2 in regulating p53 and p21 dynamics are different.

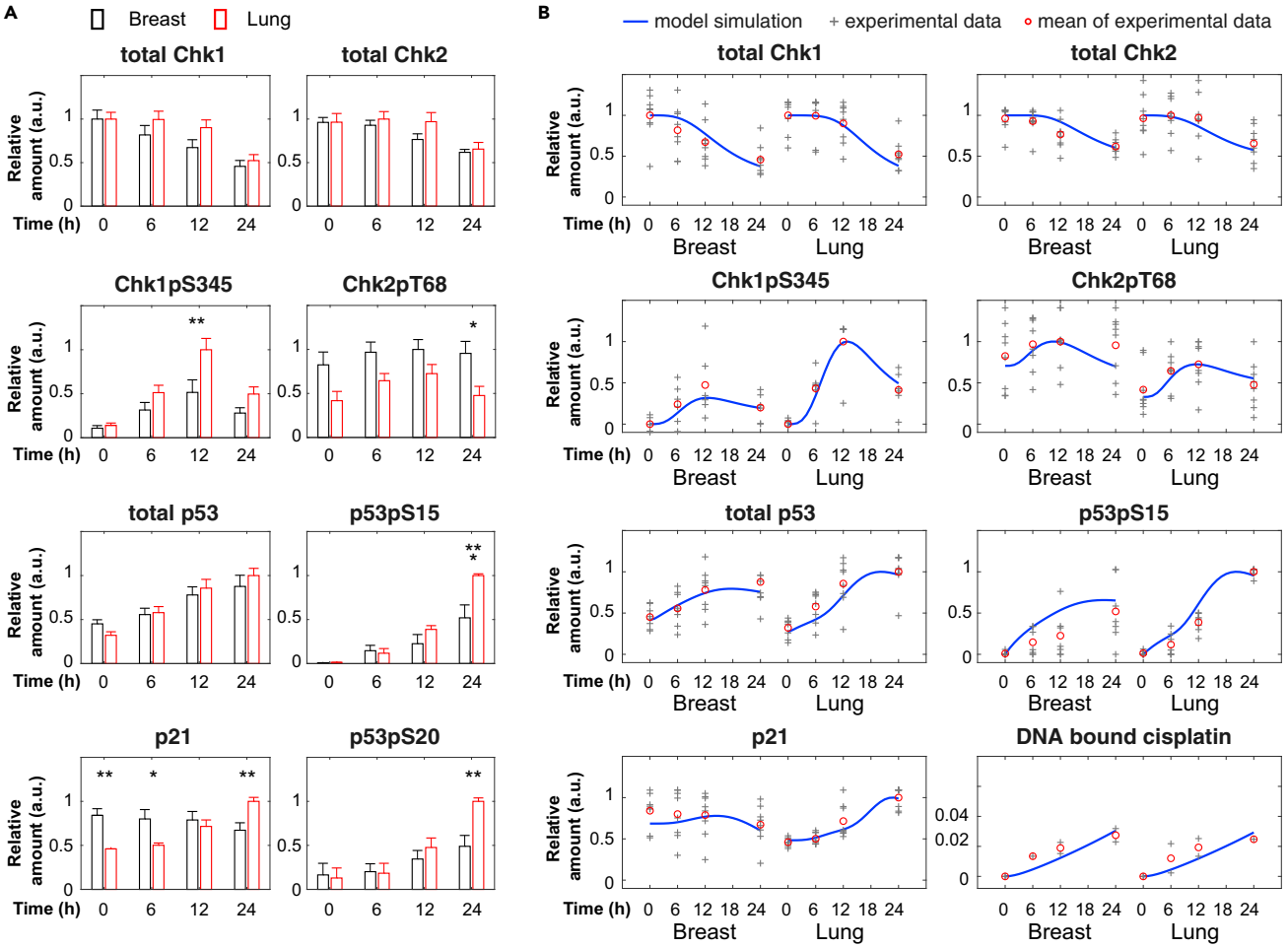

Figure 3. Cisplatin Treatment Results in Different DNA Damage Signaling Dynamics in Breast and Lung Cells

(A) Relative change of Chk1, Chk2, p53, and p21 dynamics after cisplatin treatment in breast and lung cells. Protein levels were analyzed using quantitative western blot and normalized by the number cells loaded in each sample. For every blot the highest expression value was set to 1, after which the average value was calculated for five to eight blots. Depicted is the average value normalized to the maximum value per graph. Error bars represent the SEM. Two-way ANOVAs were used to test if a protein was differentially expressed in breast versus lung cells. See also Figure S6.

(B) Comparison of model simulations to the experimental data of DNA damage signaling dynamics. To compare with the corresponding experimental data, the model simulation data were scaled as relative values (normalized to the maximal values in breast and lung cells) and depicted as blue lines. Data from individual blots are depicted as "+." The average values are shown as red circles. Note that some data points with the same values appear overlapped in this scatterplot.

To experimentally validate the model predictions, we treated breast and lung cells with inhibitors for Chk1 and Chk2, or an equivalent amount of DMSO, followed by cisplatin treatment. As predicted by the model, Chk1 inhibition did not have a significant effect on downstream targets in breast cells (Figures 4C and S10). In lung cells, however, Chk1 inhibition significantly altered p53 and p21 dynamics. Total p53 levels were unaffected, whereas p53 phosphorylation was diminished and p21 was not upregulated after cisplatin treatment (Figures 4D and S11). In line with model predictions, Chk2 inhibition resulted in the loss of p21 expression in both breast and lung cells. In addition, total and phospho-p53 levels remained low when Chk2 activity was inhibited (Figures 4C and 4D). Together, our model analyses and experimental data suggest that Chk1 activity plays a regulatory role in p53 activation, whereas Chk2 is essential for p53 activation and expression.

Breast Cells Are More Resistant to DNA Double-Strand Breaks Than Lung Cells

Chk1 is strongly activated by single-strand DNA damage, whereas Chk2 is mostly activated by DNA DSBs (Bartek and Lukas, 2003; Smith et al., 2010). We therefore wondered what happens if we treat primary breast

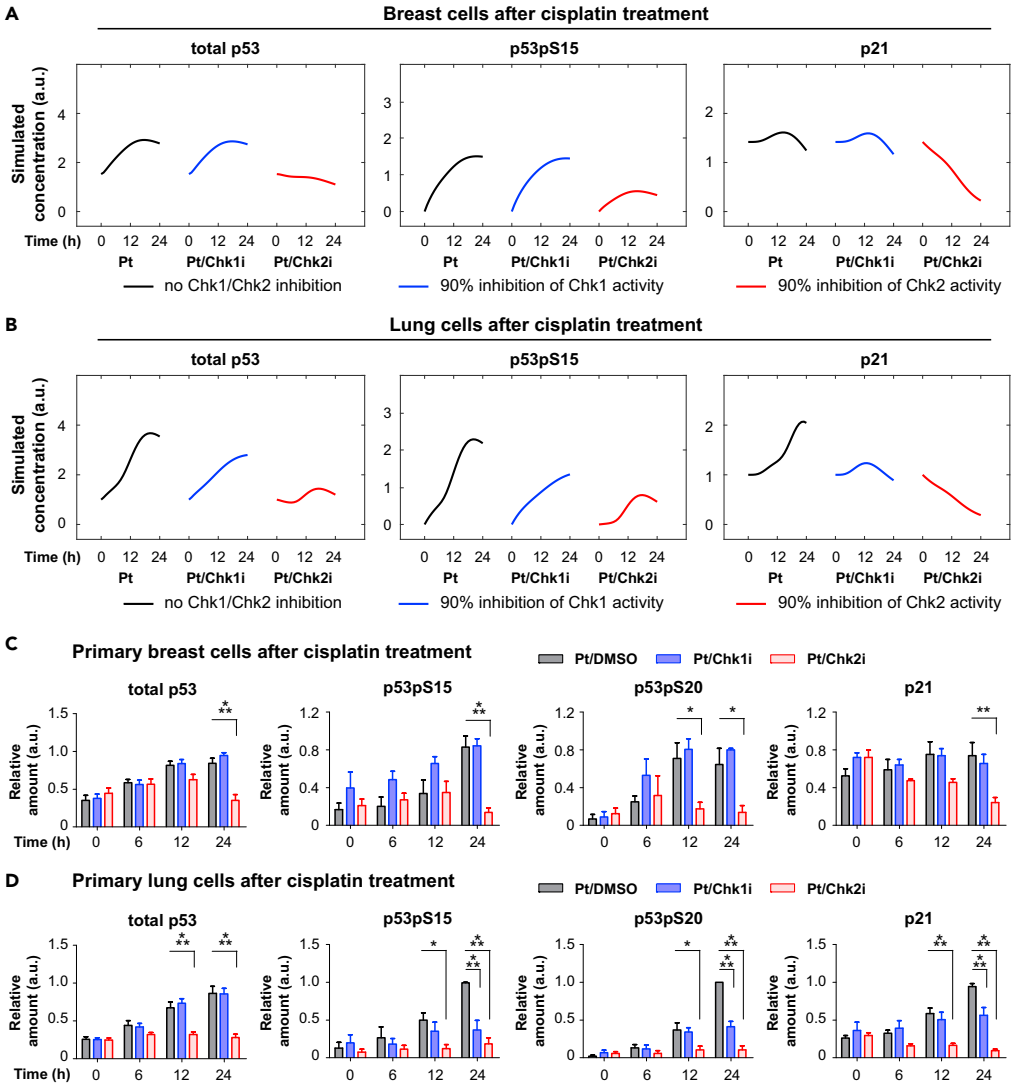

Figure 4. Inhibitor Studies Reveal Different Roles for Chk1 and Chk2 in Breast and Lung Cells

(A and B) Model predictions for the inhibition of Chk1 and Chk2 in breast (A) and lung cells (B).

(C and D) Inhibition of Chk1 and Chk2 alter p53 and p21 dynamics. Primary breast (C) and lung cells (D) were pretreated for 1 h with inhibitors against Chk1 (PF477736; 1 μM) and Chk2 (Inhibitor II, 10 μM) or an equivalent amount of DMSO, followed by cisplatin treatment. Depicted is the average relative expression (n = 3–7) for each condition normalized to the maximum value. Error bars represent the SEM. Two-way ANOVAs were used to test if a protein was differentially expressed between treatments.

See also Figures S10 and S11.

and lung cells with the DSB-inducing drug doxorubicin. Doxorubicin induces DNA adducts and also causes DNA DSBs by inhibiting topoisomerase II activity (Arcamone et al., 1969; Yang et al., 2014). When cell viability response data were plotted against the level of intracellular doxorubicin at 48 h (Figure S12), breast cells were more resistant than lung cells (Figure 5A). Surprisingly, this is opposite to the effect of cisplatin, which induces more apoptosis in breast cells, and suggests that the sensitivities of breast and lung cells to genotoxic stress depend on the nature of DNA damage.

To compare how DNA damage signaling is differently regulated after doxorubicin treatment, we quantitatively measured the dynamics of DNA-damaging signaling proteins. Interestingly, doxorubicin treatment led to strong activation of both ATM (S1981) and Chk2 (T68 and S516) in both cell types (Figures 5B and

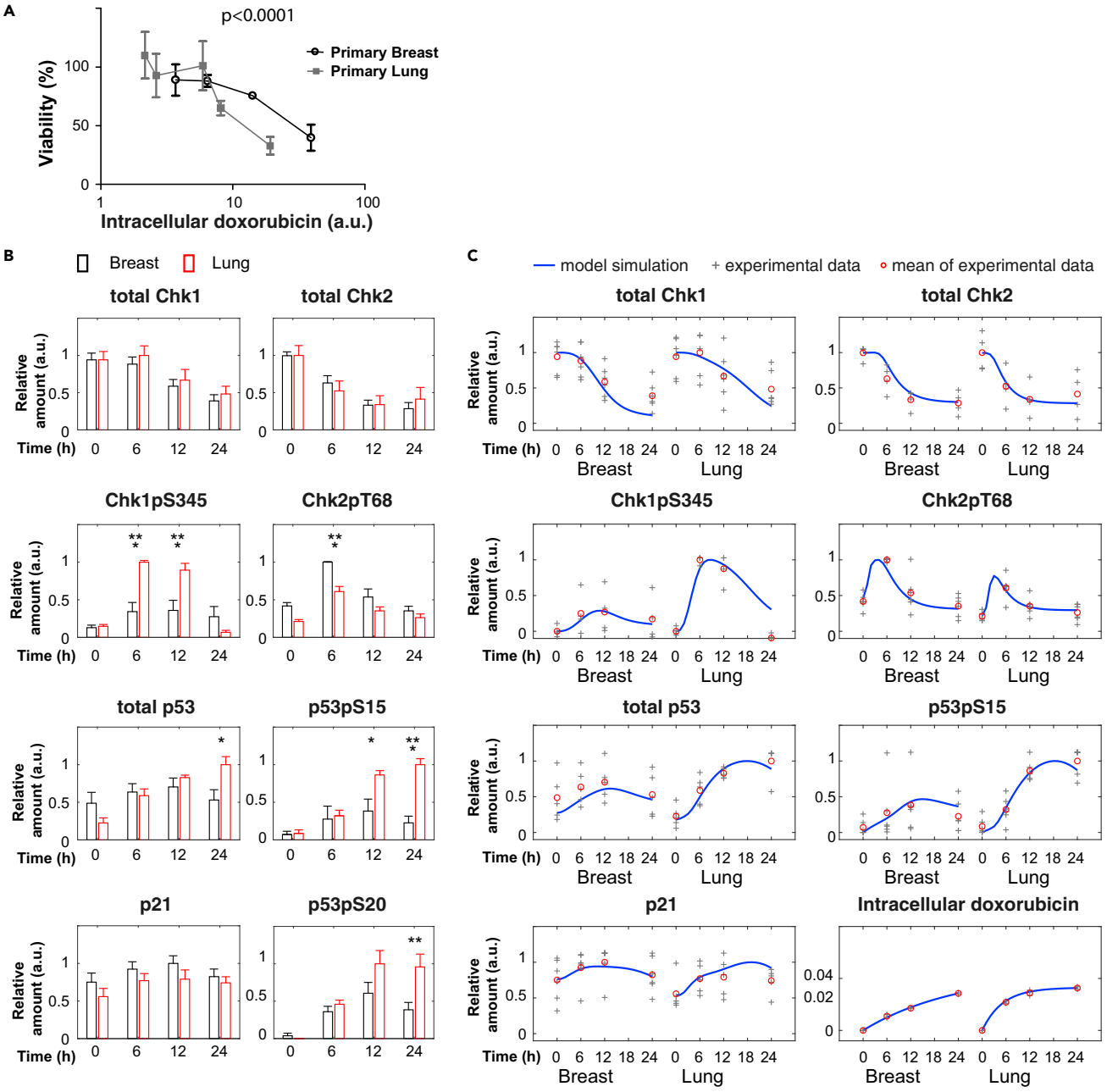

Figure 5. Breast Cells Are More Resistant to Doxorubicin Than Lung Cells

(A) Cell viability response to equal intracellular amounts of doxorubicin. After 48 h of doxorubicin treatment, intracellular doxorubicin fluorescence was determined by fluorescence-activated cell sorting (Figure S12). The intracellular doxorubicin levels (arbitrary units) were plotted against the cellular viability (as determined by MTT assay) (n = 3). Error bars represent the SD. Regression analysis was used to test if the slope and intercept were different.

(B) Relative change of Chk1, Chk2, p53, and p21 dynamics after doxorubicin treatment in breast and lung cells. Depicted is the average relative expression per treatment (n = 4–6) normalized to the maximum value per graph. Error bars represent the SEM. Two-way ANOVAs were used to test if a protein was differentially expressed in breast versus lung cells. See also Figure S13.

(C) Comparison of model simulations to the experimental data in response to doxorubicin treatment. To compare with the corresponding experimental data, the model simulation data were scaled as relative values (normalized to the maximal values in breast and lung cells) and depicted as blue lines. Data from individual blots are depicted as "+." The average values are shown as red circles. Note that some data points with the same values appear overlapped in this scatterplot.

S13), although breast cells showed higher levels of active Chk2. In addition, lung cells showed a significant higher level of ATR and Chk1 activation (S345, S317, S296) than breast cells. The induction of total and phospho-p53 was higher in lung cells, whereas p21 levels showed a weak increase in both breast and lung cells.

To understand the DDR to doxorubicin treatment, we slightly modified the values of the model parameters that are specific for cisplatin treatment. These parameters were estimated with 94 average values from 412 measured data points for doxorubicin treatment (parameters values are listed in Table S7). As shown in Figures 5C and S14, the models for doxorubicin treatment fitted well to the temporal profiles of different DNA-damage-signaling proteins in both breast and lung cells. Similar to the cisplatin model, the doxorubicin model predicted that Chk2 activity is required for p53 phosphorylation and accumulation, as well as p21 induction in both breast and lung cells (Figures S15A and S15B). Chk1 activity contributed to p53 phosphorylation, p53 accumulation, and p21 induction in lung cells. However, it has only a minor contribution in breast cells. The model predictions were confirmed by experiments with Chk1 and Chk2 inhibitors (Figures S15C, S15D, S16, and S17).

A "Friction Model" Suggests that the Balance of p53 and p21 Dynamics Contributes to Chemotherapy Responses

The different apoptotic sensitivities to cisplatin and doxorubicin are counterintuitive. Therefore, it is interesting to investigate how the same DNA-damaging core network can lead to a different apoptotic sensitivity depending on the cell type and the nature of chemotherapeutic agents. Previous studies have indicated that a threshold mechanism mediates p53 cell fate decision to induce apoptosis (Kracikova et al., 2013; Paek et al., 2016). In this work, we proposed a novel "friction model" to describe the cell apoptosis response using a coarse-grained approach, in which a hypothetical threshold mechanism is used to trigger apoptosis. The model assumes that cells undergo apoptosis when the total p53 level is higher than a certain threshold, θ. Instead of using a fixed threshold, we assume that the threshold θ is proportional to the p21 expression level as p21 can act as a negative regulator for apoptosis (Abbas and Dutta, 2009; Roninson, 2002). The dynamic threshold is analogous to the friction force exerted by a surface that resists the motion of an object, which is proportional to its mass. To move cells to apoptosis, the driving force (caused by p53) should be larger than the friction force (induced by p21). As shown in Figure S18, this simplified friction model was able to reproduce the different cell viability responses in breast and lung cells after cisplatin or doxorubicin treatment.

Additional modeling analyses indicated that the balance between p53 and p21 dynamics could explain the differential sensitivities to diverse chemotherapeutic agents. In case of cisplatin treatment, both breast and lung cells have a similar accumulation of p53 protein (similar driving forces), whereas p21 expression is induced more in lung cells. Therefore the overall friction force is larger in lung cells, which makes lung cells more resistant to apoptosis after cisplatin treatment (Figures 6A and 6B). Indeed, an inhibitor of p21 transcription could sensitize lung cells to cisplatin treatment ($p < 0.001$; Figure S19). On the other hand, after doxorubicin treatment the p53 level in lung cells is higher, whereas p21 dynamics is similar. Hence, the driving force is lower in breast cells, explaining why breast cells are more resistant (Figures 6C and 6D). In summary, the model suggests that the balance of p53 and p21 dynamics contributes to the decision to undergo apoptosis after DNA damage.

DISCUSSION

We report here that primary non-transformed breast and lung cells have different sensitivities for DNA-damaging agents. Breast cells are more sensitive to the DNA adduct and cross-linking agent cisplatin, whereas lung cells are more sensitive to the DNA adduct and DSB-inducing agent doxorubicin. These differences in sensitivity can be explained by the differential activation of Chk1, which is phosphorylated to a greater extent in lung cells. In contrast, in breast cells, Chk2 is activated to a higher extent after doxorubicin treatment. The differential activities of Chk1 and Chk2 affect p53 and p21 dynamics and hence contribute to drug sensitivity. Although differences in p53 and p21 dynamics and downstream pathways have been described in tissue-specific stem cells before (Blanpain et al., 2011; Insinga et al., 2013; Vitale et al., 2017), they were considered to be stem cell properties that change after differentiation (Insinga et al., 2013). Our study shows for the first time that healthy epithelial cell types have a different DDR. Moreover, our observation that differences in DDR can already be observed at the level of DNA damage detection is novel.

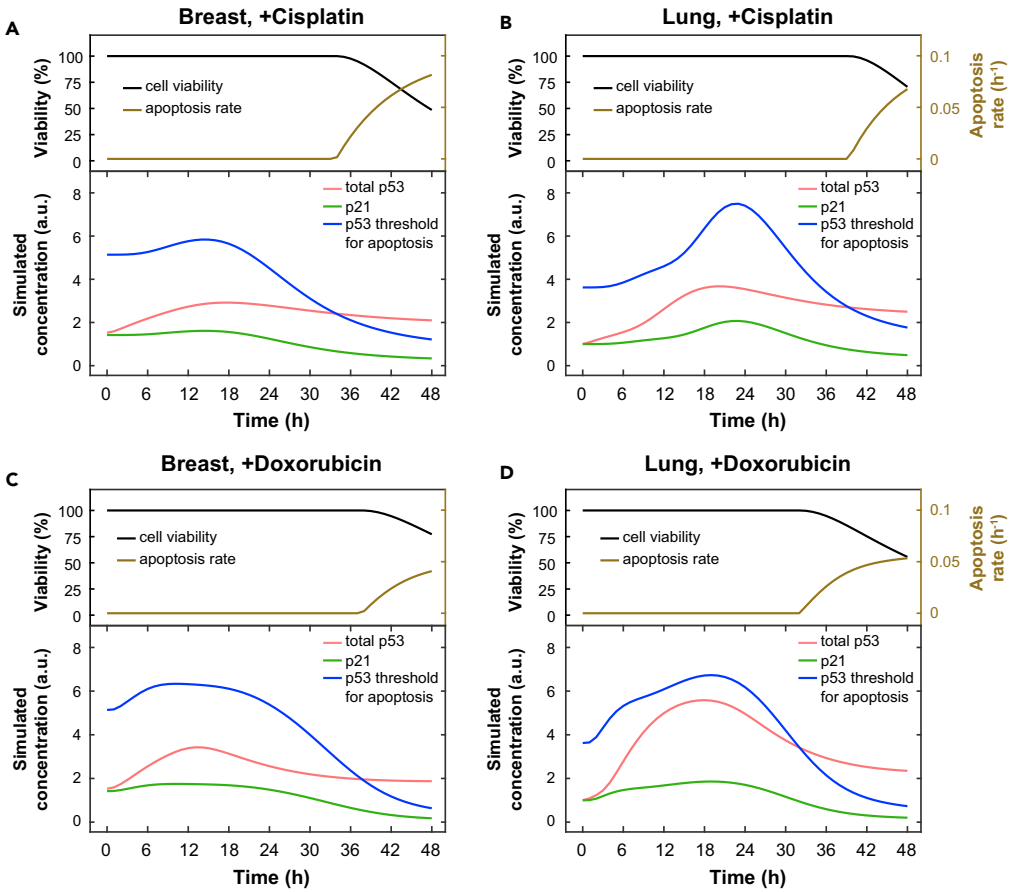

Figure 6. Mathematical Modeling Shows that the Balance of p53 and p21 Levels Determines Cell Viability after DNA Damage

(A–D) Model simulations for the dynamics of cell viability, apoptosis rate, p53, p21, and threshold for apoptosis in response to cisplatin (A and B) or doxorubicin (C and D) in breast and lung cells.

An intriguing question is why breast and lung cells show different Chk1 and Chk2 activities. The ATR-Chk1 pathway is most strongly activated by single-strand DNA damage, whereas the ATM-Chk2 pathway plays a role in DSB repair. As cell types experience different kinds of DNA damage, it may be advantageous to tailor DDR protein dynamics to the form of DNA damage that occurs most frequently. For instance, the high oxygen levels in lung likely result in increased numbers of free radicals, which can damage the DNA by causing DNA adducts and other forms of single-strand damage (Cadet and Wagner, 2013; Pham-Huy et al., 2008). This may explain why Chk1 is activated to a higher extent in lung cells than breast cells. In contrast, in breast, metabolic by-products of estrogen signaling (Yasuda et al., 2017) are known to give rise to DSBs (Savage et al., 2014), indicating that breast cells may need enhanced ATM-Chk2 signaling. The causes of the differences in Chk1 and Chk2 activities in breast and lung cells are unknown. This will be the subject of future study.

We observed that primary breast cells are more sensitive to cisplatin, and lung cells, to doxorubicin treatment. Paradoxically, first-line chemotherapeutic regimens for breast and lung cancer are mostly based on doxorubicin or cisplatin, respectively (Crown, 1998; Laskin and Sandler, 2005; Paoletti et al., 2011; von Minckwitz, 2007). It is likely that during tumorigenesis breast and lung cancer cells become more sensitive to doxorubicin and cisplatin, respectively, as breast cancer cell lines respond well to doxorubicin and non-small-cell lung cancer cell lines are generally sensitive to cisplatin (Alley et al., 1988; Shoemaker, 2006). The goal of cancer therapy is to destroy cancer cells while sparing healthy cells. The difference in sensitivity between normal and transformed cells would provide a window to selectively kill cancer cells. It would be interesting to investigate if and how the sensitivity for DNA damage changes during tumorigenesis.

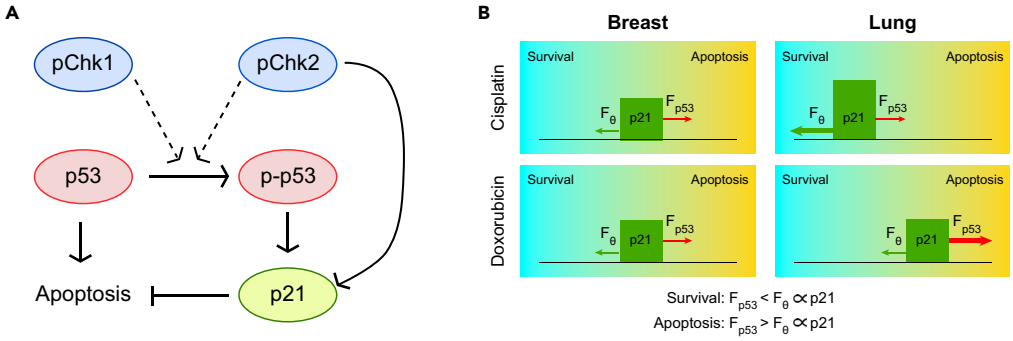

Figure 7. A Friction Model of Cell Apoptosis Response to DNA Damage Signaling

(A) A simple scheme for Chk1, Chk2, p53, and p21 protein interactions.

(B) A cartoon of the "friction model." A cyan-to-orange gradient indicates the balance between survival (cyan region) and apoptosis (orange region). Cellular outcome to DNA damage is determined by the balance of the driving force (caused by p53) and the friction force (induced by p21). To move cells to the apoptotic state, the driving force should be larger than the friction force. The size of arrows depicts the relative strength of the driving and friction forces in breast and lung cells in response to cisplatin or doxorubicin treatment. p-Chk1 and p-Chk2 contribute to p53 phosphorylation, and both p-p53 and Chk2 can induce p21 transcription. However, whether p21 expression increases also depends on the nature of the stress.

Chk1 inhibitors have recently attracted attention as sensitizers for chemotherapy as Chk1 is frequently overexpressed in tumors (Zhang and Hunter, 2014). Our model confirms that Chk1 overexpression could lead to increased cisplatin resistance and hence provides a rationale for co-treatment of Chk1 inhibitors with cisplatin. Indeed, Chk1 inhibition has been found to decrease cisplatin resistance in cancer cell lines (Gadhikar et al., 2013; Li et al., 2016; Thompson et al., 2012). However, the observation that Chk1 inhibition did not sensitize breast cells to cisplatin may indicate that only tumors with overactive Chk1 may respond to Chk1 inhibition, and hence calls for careful patient stratification in clinical trials.

Both ATR-Chk1 and ATM-Chk2 signaling are known to regulate p53 stabilization and phosphorylation. Our model predicts that Chk1 and Chk2 affect p53 dynamics differently. Chk2 activity is required for p53 phosphorylation, whereas Chk1 activity is not essential, but contributes to p53 phosphorylation (Figure 7A). As a consequence of its higher activity in lung cells, Chk1 contributes to p53 phosphorylation in lung cells but not in breast cells. As expected, a Chk1 inhibitor reduced p53 phosphorylation levels only in lung cells. Although Chk1 has been demonstrated to be able to phosphorylate p53 on S15 and S20 (Shieh et al., 2000), some studies reported that Chk1 inhibition did not diminish p53 phosphorylation (Tian et al., 2002; Wu et al., 2013). Our data indicate that this may be a cell-type or DNA-damage-specific effect.

We propose a "friction model" to explain the differences in apoptotic sensitivity for cisplatin and doxorubicin in breast and lung cells. The induction of apoptosis is a complex process that may involve caspase-dependent or caspase-independent pathways and is regulated by pro- and anti-survival proteins. We did not incorporate these effects in our model because we found that a simplified version of apoptosis induction, based on the balance between p53 and p21 dynamics, was sufficient to explain the apoptotic response. Moreover, additional processes will increase the complexity of the model, and studying these detailed regulations is not the focus of this work. Our new friction model incorporates the idea of a dynamic p53 threshold for apoptosis induction (Paek et al., 2016), but defines it as a function of p21 levels. After cisplatin treatment, p53 dynamics are similar in breast and lung cells causing a similar apoptotic stimulus (Figure 7B). The difference in cisplatin resistance can be explained because in lung cells increased amounts of p53 phosphorylation (as result of increased Chk1 activity) give rise to p21 induction, resulting in an increased apoptotic threshold. In contrast, after doxorubicin treatment p21 dynamics are similar in breast and lung cells. In this case, increased p53 phosphorylation in lung cells leads to stabilization of p53, which translates into a higher apoptotic stimulus and enhanced sensitivity to doxorubicin (Figure 7B). A possible role for p21 as a friction force is supported by data for the p21 inhibitor UC2288. Although the mechanism of action of this inhibitor is incompletely understood, we observed down-regulation of p21 after treatment. We cannot exclude, however, that the role of p21 is cellular context dependent. In addition, it is likely that other proteins could contribute to the friction

force as well, such as the inhibitors of apoptosis (IAP) family proteins (Deveraux and Reed, 1999; Paek et al., 2016).

In summary, our study provides new insights into the apoptotic sensitivity for DNA-damaging agents. It will be interesting to investigate how modulating Chk1 levels and the balance between p53 and p21 may improve the effectiveness of chemotherapy.

Limitations of the Study

In this study we made use of primary epithelial cells to investigate the DDR in healthy cells. Although this study provided novel insights into how Chk1, Chk2, p53, and p21 collectively affect the apoptotic response to DNA-damaging chemotherapy in different tissues, subsequent studies are necessary to investigate the implication for cancer cells and cancer treatment. In addition, in this study, we described a friction model to explain the difference in apoptotic sensitivity between breast and lung cells for two different anti-cancer drugs. This friction model is based on the balance of p53 and p21. It is likely, however, that other anti-apoptotic proteins (such as the IAP family of proteins) could contribute to the friction force as well. Furthermore, in our mathematical model, different p53 negative regulators are lumped as one abstract variable "negative feedback regulator", which makes it difficult to study the contributions of specific negative regulators. As different p53 negative regulators may affect p53 expression and activity in different ways, their exact roles and contributions need to be further studied.

METHODS

All methods can be found in the accompanying Transparent Methods supplemental file.

SUPPLEMENTAL INFORMATION

Supplemental Information includes Transparent Methods, 19 figures, and 7 tables and can be found with this article online at https://doi.org/10.1016/j.isci.2019.01.001.

ACKNOWLEDGMENTS

We would like to thank Joris Pothof, Maikel Wouters, and Serena Bruens for providing cell line samples; Peter de Bruijn for measuring platinum concentrations in DNA samples; Uta Marchfelder for setting up the FACS; and Susanne Freier for help in experiments. We are also grateful to Alexander Meissner for his critical reading of this manuscript. This work was supported by a grant to Z.Z. from the Federal Ministry of Education and Research (BMBF, Germany) within the e:Bio project (031A309).

AUTHOR CONTRIBUTIONS

M.T.v.J. designed and performed the experiments; Z.Z. developed the mathematical model and performed modeling analyses; D.D. assisted at the western blot experiments; and E.A.C.W. provided insights and commented on the results. M.T.v.J. and Z.Z. analyzed the data and wrote the manuscript. Z.Z. supervised the project.

DECLARATION OF INTERESTS

The authors declare no competing interests.

Received: July 27, 2018
Revised: October 16, 2018
Accepted: December 31, 2018
Published: February 22, 2019

REFERENCES

Abbas, T., and Dutta, A. (2009). p21 in cancer: intricate networks and multiple activities. Nat. Rev. Cancer *9*, 400–414.

Alexandrov, L.B., Nik-Zainal, S., Wedge, D.C., Aparicio, S.A., Behjati, S., Biankin, A.V., Bignell, G.R., Bolli, N., Borg, A., Borresen-Dale, A.L., et al. (2013). Signatures of mutational processes in human cancer. Nature *500*, 415–421.

Alley, M.C., Scudiero, D.A., Monks, A., Hursey, M.L., Czerwinski, M.J., Fine, D.L., Abbott, B.J., Mayo, J.G., Shoemaker, R.H., and Boyd, M.R. (1988). Feasibility of drug screening with panels of human tumor cell lines using a microculture tetrazolium assay. Cancer Res. *48*, 589–601.

Arcamone, F., Cassinelli, G., Fantini, G., Grein, A., Orezzi, P., Pol, C., and Spalla, C. (1969). Adriamycin, 14-hydroxydaunomycin, a new

antitumor antibiotic from *S. peucetius* var. caesius. Biotechnol. Bioeng. *11*, 1101–1110.

Barr, A.R., Cooper, S., Heldt, F.S., Butera, F., Stoy, H., Mansfeld, J., Novak, B., and Bakal, C. (2017). DNA damage during S-phase mediates the proliferation-quiescence decision in the subsequent G1 via p21 expression. Nat. Commun. *8*, 14728.

Bartek, J., and Lukas, J. (2003). Chk1 and Chk2 kinases in checkpoint control and cancer. Cancer Cell *3*, 421–429.

Batchelor, E., Mock, C.S., Bhan, I., Loewer, A., and Lahav, G. (2008). Recurrent initiation: a mechanism for triggering p53 pulses in response to DNA damage. Mol. Cell *30*, 277–289.

Batchelor, E., Loewer, A., Mock, C., and Lahav, G. (2011). Stimulus-dependent dynamics of p53 in single cells. Mol. Syst. Biol. *7*, 488.

Blanpain, C., Mohrin, M., Sotiropoulou, P.A., and Passegue, E. (2011). DNA-damage response in tissue-specific and cancer stem cells. Cell Stem Cell *8*, 16–29.

Cadet, J., and Wagner, J.R. (2013). DNA base damage by reactive oxygen species, oxidizing agents, and UV radiation. Cold Spring Harb. Perspect. Biol. *5*, a012559.

Chae, Y.K., Anker, J.F., Carneiro, B.A., Chandra, S., Kaplan, J., Kalyan, A., Santa-Maria, C.A., Platanias, L.C., and Giles, F.J. (2016). Genomic landscape of DNA repair genes in cancer. Oncotarget *7*, 23312–23321.

Crown, J. (1998). Evolution in the treatment of advanced breast cancer. Semin. Oncol. *25*, 12–17.

Deveraux, Q.L., and Reed, J.C. (1999). IAP family proteins–suppressors of apoptosis. Genes Dev. *13*, 239–252.

Eastman, A. (1987). The formation, isolation and characterization of DNA adducts produced by anticancer platinum complexes. Pharmacol. Ther. *34*, 155–166.

Forestier, A., Sarrazy, F., Caillat, S., Vandenbrouck, Y., and Sauvaigo, S. (2012). Functional DNA repair signature of cancer cell lines exposed to a set of cytotoxic anticancer drugs using a multiplexed enzymatic repair assay on biochip. PLoS One *7*, e51754.

Gadhikar, M.A., Sciuto, M.R., Alves, M.V., Pickering, C.R., Osman, A.A., Neskey, D.M., Zhao, M., Fitzgerald, A.L., Myers, J.N., and Frederick, M.J. (2013). Chk1/2 inhibition overcomes the cisplatin resistance of head and neck cancer cells secondary to the loss of functional p53. Mol. Cancer Ther. *12*, 1860–1873.

Garner, K.M., and Eastman, A. (2011). Variations in Mre11/Rad50/Nbs1 status and DNA damage-induced S-phase arrest in the cell lines of the NCI60 panel. BMC Cancer *11*, 201–213.

Gettinger, S., and Lynch, T. (2011). A decade of advances in treatment for advanced non-small cell lung cancer. Clin. Chest Med. *32*, 839–851.

Hoeijmakers, J.H. (2009). DNA damage, aging, and cancer. N. Engl. J. Med. *361*, 1475–1485.

Hu, J., Lieb, J.D., Sancar, A., and Adar, S. (2016). Cisplatin DNA damage and repair maps of the human genome at single-nucleotide resolution. Proc. Natl. Acad. Sci. U S A *113*, 11507–11512.

Insinga, A., Cicalese, A., Faretta, M., Gallo, B., Albano, L., Ronzoni, S., Furia, L., Viale, A., and Pelicci, P.G. (2013). DNA damage in stem cells activates p21, inhibits p53, and induces symmetric self-renewing divisions. Proc. Natl. Acad. Sci. U S A *110*, 3931–3936.

Kandoth, C., McLellan, M.D., Vandin, F., Ye, K., Niu, B., Lu, C., Xie, M., Zhang, Q., McMichael, J.F., Wyczalkowski, M.A., et al. (2013). Mutational landscape and significance across 12 major cancer types. Nature *502*, 333–339.

Kracikova, M., Akiri, G., George, A., Sachidanandam, R., and Aaronson, S.A. (2013). A threshold mechanism mediates p53 cell fate decision between growth arrest and apoptosis. Cell Death Differ. *20*, 576–588.

Laskin, J.J., and Sandler, A.B. (2005). First-line treatment for advanced non-small-cell lung cancer. Oncology (Williston Park) *19*, 1671–1676, discussion 1678–1680.

Levy-Lahad, E., and Friedman, E. (2007). Cancer risks among BRCA1 and BRCA2 mutation carriers. Br. J. Cancer *96*, 11–15.

Li, C.C., Yang, J.C., Lu, M.C., Lee, C.L., Peng, C.Y., Hsu, W.Y., Dai, Y.H., Chang, F.R., Zhang, D.Y., Wu, W.J., et al. (2016). ATR-Chk1 signaling inhibition as a therapeutic strategy to enhance cisplatin chemosensitivity in urothelial bladder cancer. Oncotarget *7*, 1947–1959.

Liu, C., Chang, H., Li, X.H., Qi, Y.F., Wang, J.O., Zhang, Y., and Yang, X.H. (2017). Network meta-analysis on the effects of DNA damage response-related gene mutations on overall survival of breast cancer based on TCGA database. J. Cell Biochem. *118*, 4728–4734.

Ma, L., Wagner, J., Rice, J.J., Hu, W., Levine, A.J., and Stolovitzky, G.A. (2005). A plausible model for the digital response of p53 to DNA damage. Proc. Natl. Acad. Sci. U S A *102*, 14266–14271.

Michailidou, K., Lindstrom, S., Dennis, J., Beesley, J., Hui, S., Kar, S., Lemacon, A., Soucy, P., Glubb, D., Rostamianfar, A., et al. (2017). Association analysis identifies 65 new breast cancer risk loci. Nature *551*, 92–94.

von Minckwitz, G. (2007). Docetaxel/anthracycline combinations for breast cancer treatment. Expert Opin. Pharmacother. *8*, 485–495.

Nevanlinna, H., and Bartek, J. (2006). The CHEK2 gene and inherited breast cancer susceptibility. Oncogene *25*, 5912–5919.

Non-small Cell Lung Cancer Collaborative Group (1995). Chemotherapy in non-small cell lung cancer: a meta-analysis using updated data on individual patients from 52 randomised clinical trials. BMJ *311*, 899–909.

Paek, A.L., Liu, J.C., Loewer, A., Forrester, W.C., and Lahav, G. (2016). Cell-to-cell variation in p53 dynamics leads to fractional killing. Cell *165*, 631–642.

Paoletti, L., Pastis, N.J., Denlinger, C.E., and Silvestri, G.A. (2011). A decade of advances in treatment of early-stage lung cancer. Clin. Chest Med. *32*, 827–838.

Pham-Huy, L.A., He, H., and Pham-Huy, C. (2008). Free radicals, antioxidants in disease and health. Int. J. Biomed. Sci. *4*, 89–96.

Reinhardt, H.C., and Schumacher, B. (2012). The p53 network: cellular and systemic DNA damage responses in aging and cancer. Trends Genet. *28*, 128–136.

Roninson, I.B. (2002). Oncogenic functions of tumour suppressor p21(Waf1/Cip1/Sdi1): association with cell senescence and tumour-promoting activities of stromal fibroblasts. Cancer Lett. *179*, 1–14.

Rosenberg, B., VanCamp, L., Trosko, J.E., and Mansour, V.H. (1969). Platinum compounds: a new class of potent antitumour agents. Nature *222*, 385–386.

Savage, K.I., Matchett, K.B., Barros, E.M., Cooper, K.M., Irwin, G.W., Gorski, J.J., Orr, K.S., Vohhodina, J., Kavanagh, J.N., Madden, A.F., et al. (2014). BRCA1 deficiency exacerbates estrogen-induced DNA damage and genomic instability. Cancer Res. *74*, 2773–2784.

Shieh, S.Y., Ahn, J., Tamai, K., Taya, Y., and Prives, C. (2000). The human homologs of checkpoint kinases Chk1 and Cds1 (Chk2) phosphorylate p53 at multiple DNA damage-inducible sites. Genes Dev. *14*, 289–300.

Shoemaker, R.H. (2006). The NCI60 human tumour cell line anticancer drug screen. Nat. Rev. Cancer *6*, 813–823.

Smith, J., Tho, L.M., Xu, N., and Gillespie, D.A. (2010). The ATM-Chk2 and ATR-Chk1 pathways in DNA damage signaling and cancer. Adv. Cancer Res. *108*, 73–112.

Sousa, F.G., Matuo, R., Tang, S.W., Rajapakse, V.N., Luna, A., Sander, C., Varma, S., Simon, P.H., Doroshow, J.H., Reinhold, W.C., et al. (2015). Alterations of DNA repair genes in the NCI-60 cell lines and their predictive value for anticancer drug activity. DNA Repair (Amst) *28*, 107–115.

Stewart-Ornstein, J., and Lahav, G. (2017). p53 dynamics in response to DNA damage vary across cell lines and are shaped by efficiency of DNA repair and activity of the kinase ATM. Sci. Signal. *10*, eaah6671.

Thompson, R., Meuth, M., Woll, P., Zhu, Y., and Danson, S. (2012). Treatment with the Chk1 inhibitor Go6976 enhances cisplatin cytotoxicity in SCLC cells. Int. J. Oncol. *40*, 194–202.

Tian, H., Faje, A.T., Lee, S.L., and Jorgensen, T.J. (2002). Radiation-induced phosphorylation of Chk1 at S345 is associated with p53-dependent cell cycle arrest pathways. Neoplasia *4*, 171–180.

Vitale, I., Manic, G., De Maria, R., Kroemer, G., and Galluzzi, L. (2017). DNA damage in stem cells. Mol. Cell *66*, 306–319.

Weber, A.M., and Ryan, A.J. (2015). ATM and ATR as therapeutic targets in cancer. Pharmacol. Ther. *149*, 124–138.

Wu, G., Lin, N., Xu, L., Liu, B., and Feitelson, M.A. (2013). UCN-01 induces S and G2/M cell cycle arrest through the p53/p21(waf1) or CHK2/CDC25C pathways and can suppress invasion in human hepatoma cell lines. BMC Cancer *13*, 167.

Yang, F., Teves, S.S., Kemp, C.J., and Henikoff, S. (2014). Doxorubicin, DNA torsion, and chromatin dynamics. Biochim. Biophys. Acta *1845*, 84–89.

Yasuda, M.T., Sakakibara, H., and Shimoi, K. (2017). Estrogen- and stress-induced DNA damage in breast cancer and chemoprevention with dietary flavonoid. Genes Environ. *39*, 10.

Zehir, A., Benayed, R., Shah, R.H., Syed, A., Middha, S., Kim, H.R., Srinivasan, P., Gao, J., Chakravarty, D., Devlin, S.M., et al. (2017). Mutational landscape of metastatic cancer revealed from prospective clinical sequencing of 10,000 patients. Nat. Med. *23*, 703–713.

Zhang, Y., and Hunter, T. (2014). Roles of Chk1 in cell biology and cancer therapy. Int. J. Cancer *134*, 1013–1023.

Zhang, X.P., Liu, F., and Wang, W. (2011). Two-phase dynamics of p53 in the DNA damage response. Proc. Natl. Acad. Sci. U S A *108*, 8990–8995.

ISCI, Volume *12*

Supplemental Information

Tissue-Specific Chk1 Activation Determines Apoptosis by Regulating the Balance of p53 and p21

Marijn T.M. van Jaarsveld, Difan Deng, Erik A.C. Wiemer, and Zhike Zi

Supplemental Figures and Legends

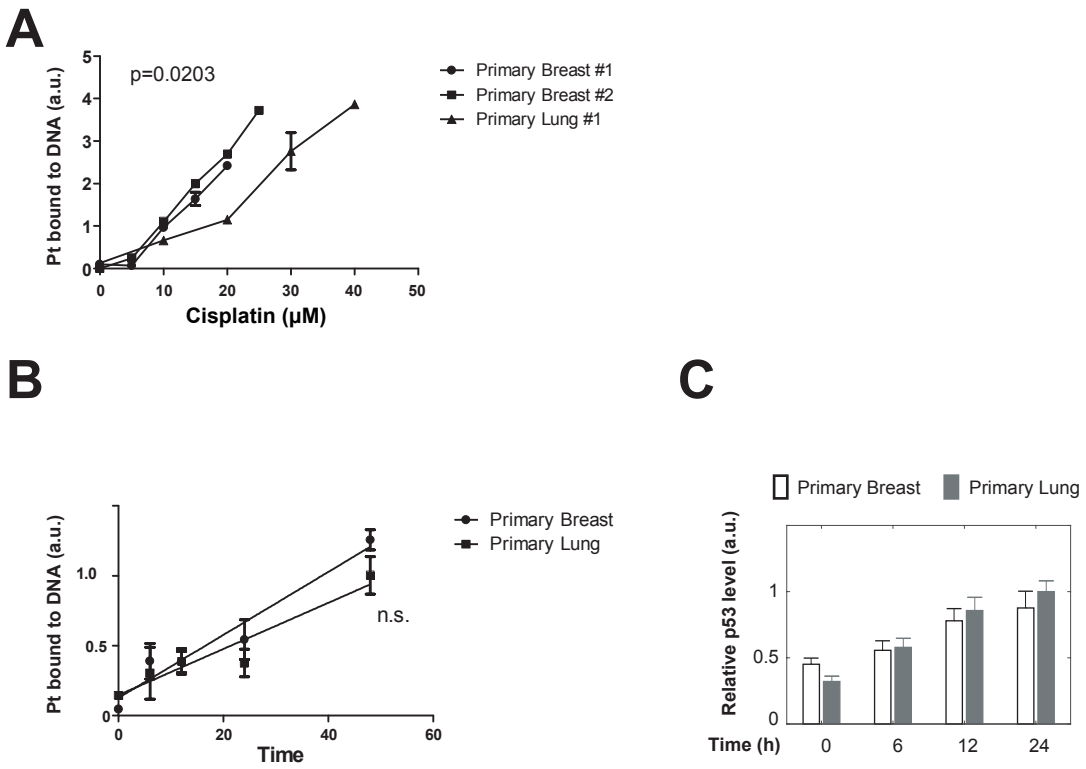

Figure S1: Treatment of breast and lung cells with 20 μM or 30 μM cisplatin induces an equal amount of Pt-DNA lesions and similar p53 kinetics, Related to Figure 1.

(A) Amount of DNA damage (pg Platinum/ng DNA) after cisplatin treatment in breast cells and lung cells (n=2). Regression analysis was used to assess if there were differences in slope and intercept.

(B) Accumulation of DNA damage (pg platinum/ng DNA) over time after treatment of primary breast cells with 20 μM cisplatin and primary lung cells with 30 μM cisplatin (n=2). Regression analysis was used to assess if differences in slope and intercept were significant (n.s. = not significant)

(C) Time course of p53 dynamics in lung and breast cells after cisplatin treatment. Breast cells were treated with 20 μM cisplatin, and lung cells with 30 μM cisplatin. Protein levels were corrected for cell number (n=8). A two way ANOVA with Bonferroni post-hoc test was carried out to assess if differences were significant.

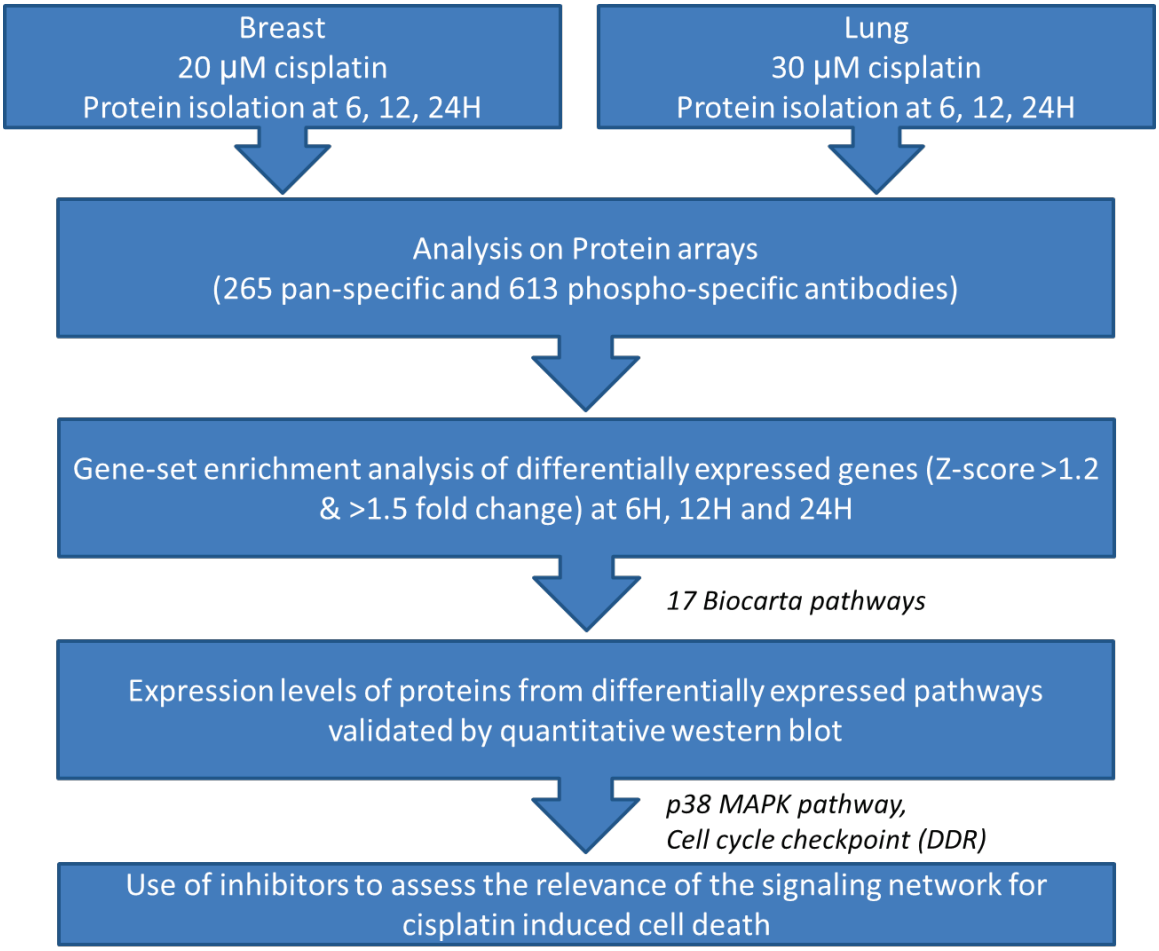

Figure S2: Proteomic profiling of the cisplatin response in primary breast and lung cells, Related to Figure 2. Breast and lung cells were treated with a cisplatin dose that causes an equal amount of damage (20 µM and 30 µM respectively). Proteins were isolated after 6h, 12h and 24h and prepared for analysis on protein array KAM-900P (Kinexus Bioinformatics). After image quantification and quantile normalization (raw data is in Table S1), proteins were identified as differentially expressed if they displayed a Z-score ratio >1.2 and a fold-change >1.5. Gene set enrichment analysis (David) of differentially expressed proteins in breast vs. lung cells revealed 17 Biocarta pathways to be significantly enriched (Figure 2A; Table S2). For differentially expressed proteins, antibody specificity was assessed by western blot. In case of a positive result, the pathway activity was measured by quantitative western blot (Figure 2C; Figure S3). To assess if differences were functionally related to cisplatin resistance, we made use of inhibitors (Figure 2D, Figure S4).

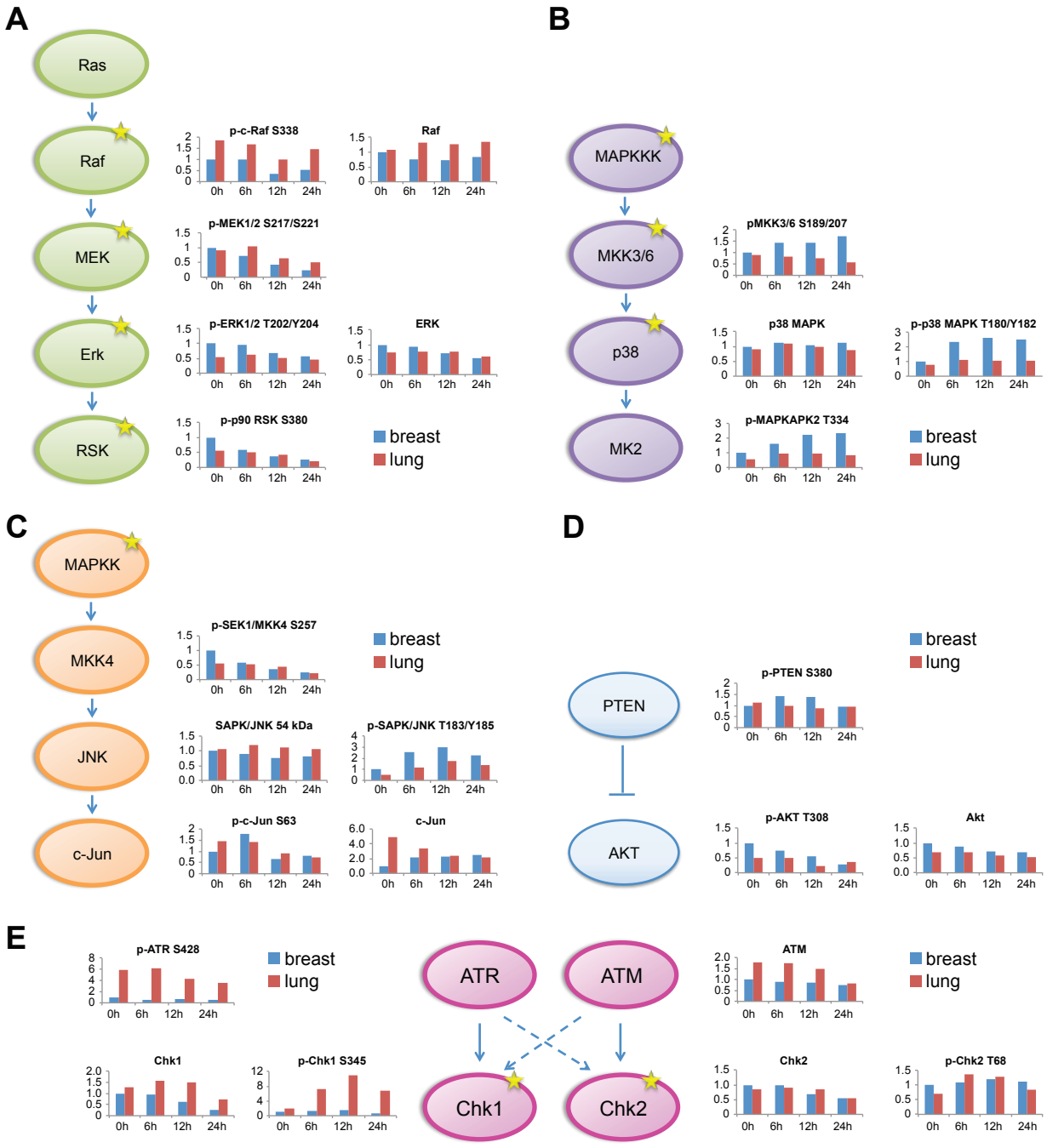

Figure S3: Validation of differentially expressed pathways by quantitative western blot, Related to Figure 2. After determining specificity of antibodies of the array (a star indicates a differentially expressed protein), quantitative western blot was performed to measure activity of differentially expressed pathways (Table S2). Expression of (phospho) proteins was normalized to β-actin. The graphs depict the result of a representative experiment (n=4). The blue bar represents the protein expression in breast cells, the red bar the protein expression in lung cells. **(A)** Ras/ERK signaling. **(B)** p38 MAPK signaling. (**C**) JNK signaling. (**D**) PTEN/Akt signaling. (**E**) DNA damage checkpoint.

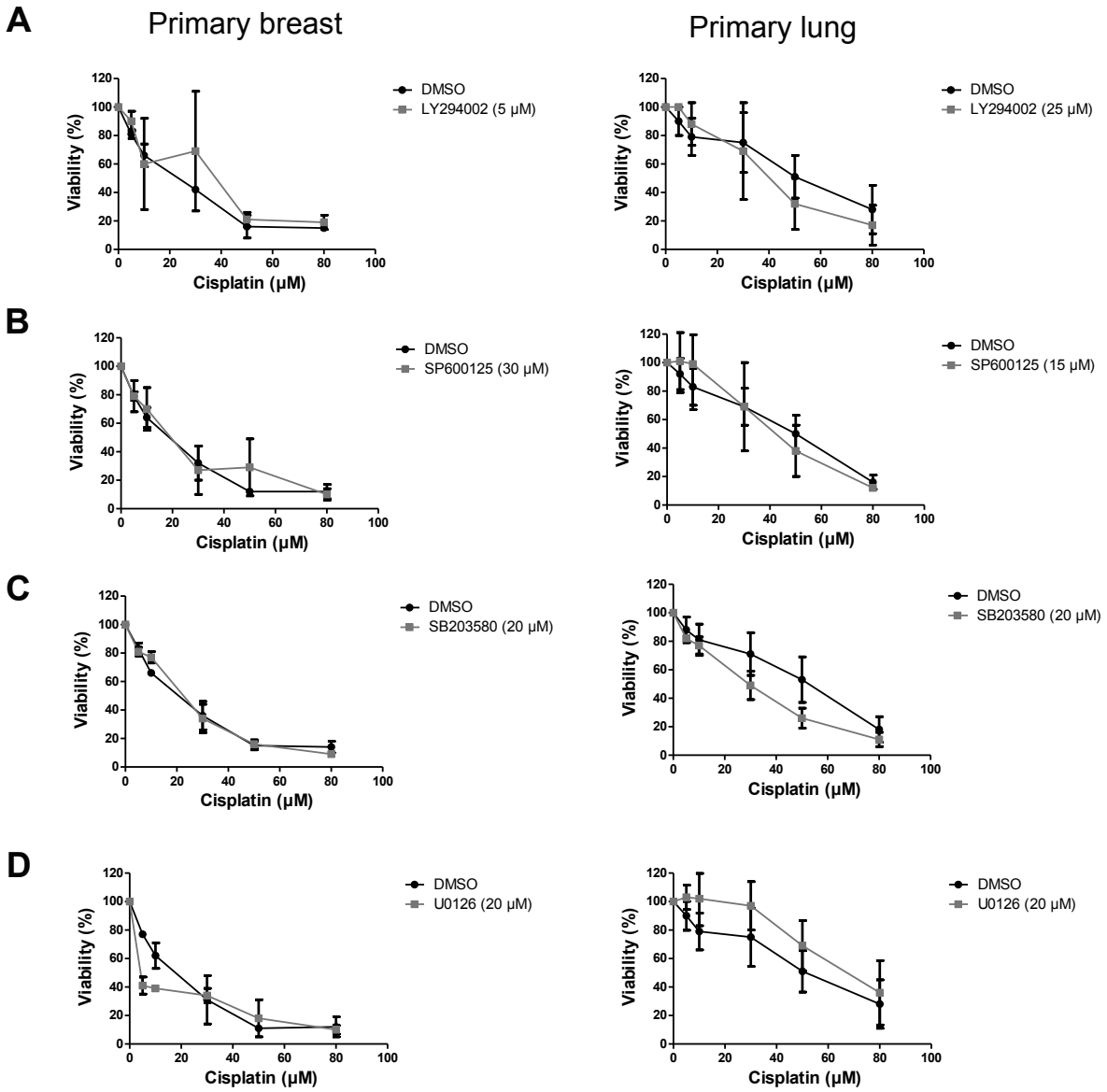

Figure S4: Inhibition of differentially expressed pathways, Related to Figure 2. Primary breast and lung cells were treated for 1 hour with an IC25 dose of inhibitor after which cisplatin was added after 48 hours, viability was determined. **(A)** PI3K (LY294002, 5 or 25 μM), **(C)** JNK kinase (SP600125, 15 or 30 μM), **(D)** p38 MAPK (SB203580, 20 μM) or **(E)** MEK (U0126, 20 μM). Error bars represent SD (n=3). Two way ANOVA's with Bonferroni post-hoc tests were carried out to assess if differences were significant.

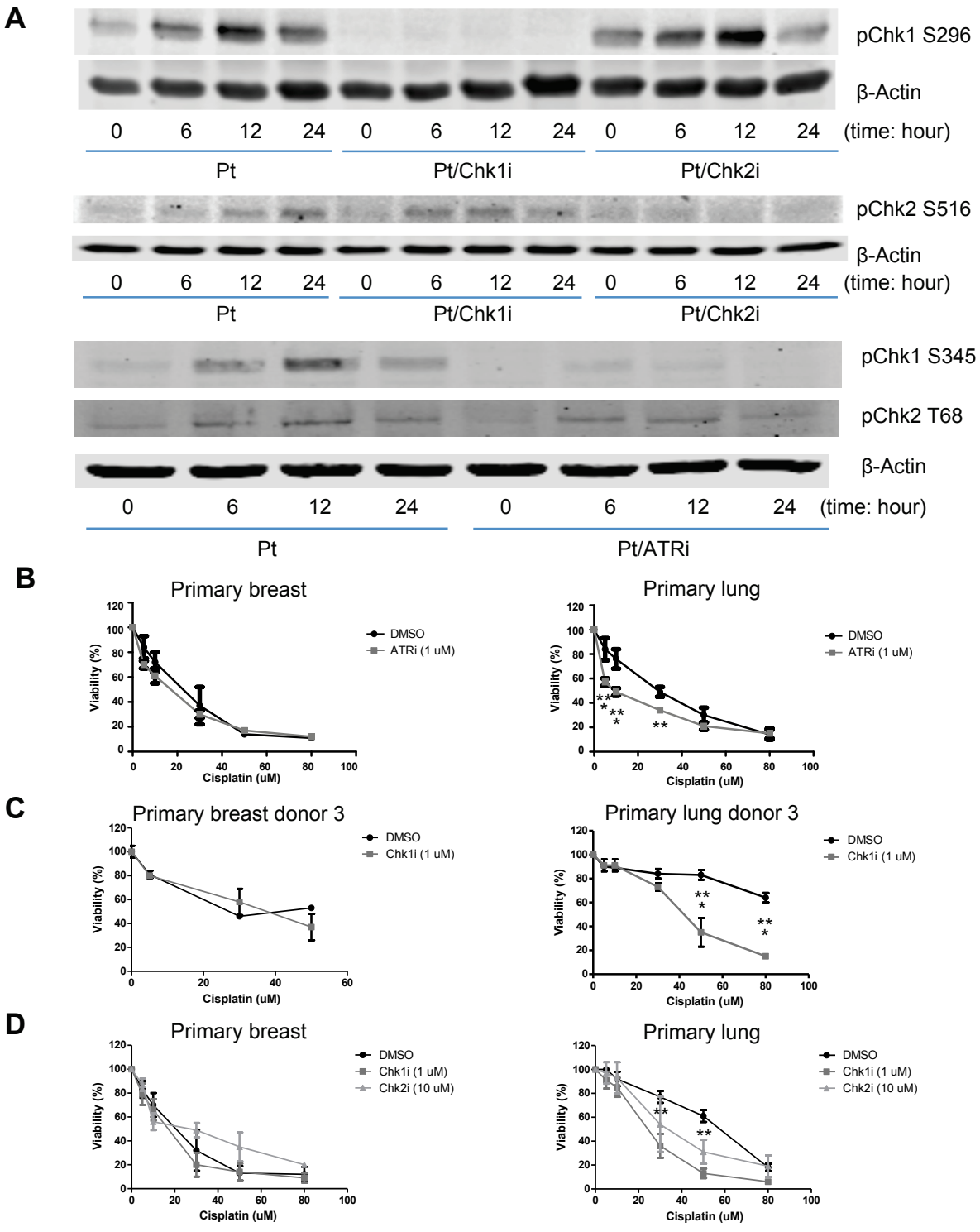

Figure S5: Effect inhibitors Chk1/Chk2 pathway, Related to Figure 2.

(A) Expression levels of active Chk1 and Chk2 after inhibitor treatment. Primary lung cells were treated with DMSO, Chk1 inhibitor (PF477736; 1 µM), Chk2 inhibitor (Chk2 inhibitor II; 10 µM) or ATR inhibitor (1 µM VE822) for 1 hour, after which 30 µM cisplatin was added to the medium, and lysates were made at the indicated time points. Since inhibitors act downstream of initial phosphorylation sites pChk1 S345 and pChk2 T68, blots were probed for pChk1 S296 (autophosphorylation site of Chk1) and pChk2 S516 (autophosphorylation site of Chk2), as markers of Chk1 and Chk2 activity.

(B) An ATR inhibitor enhances cisplatin sensitivity in primary lung cells, but not in primary breast cells. Breast and lung cells were treated with 1 μM VE822 (aka VX970) for 1 hour, followed by cisplatin treatment. After 48 hours, viability was determined. Depicted are the average values of three biological replicates. Error bars represent the standard deviation. A two-way ANOVA with Bonferroni post-hoc test was carried out to assess if differences were significant. (**=$p<0.01$; ***=$p<0.001$).

(C) Validation of effect Chk1 inhibition in primary breast and lung cells from different donors. Cells were treated for 1 hour with 1 μM PF477736 after which cisplatin was added, and after 48h viability was determined. Depicted is a representative experiment (N=3), error bars represent the SD. A two way ANOVA with Bonferroni post-hoc test was carried out to assess if differences were significant (***=$p<0.001$).

(D) Effect of Chk1/Chk2 inhibition in primary breast and lung cells. Cells were treated for 1 hour with 1 μM PF477736 or 10 μM Chk2 inhibitor II after which cisplatin was added, and after 48h viability was determined. Depicted is the average expression (N=4), error bars represent the SD. Two way ANOVAs with Bonferroni post-hoc tests were carried out to assess if differences were significant. The comparison of Chk1i vs. DMSO and Chk2i vs. DMSO yielded the same results (**=$p<0.01$).

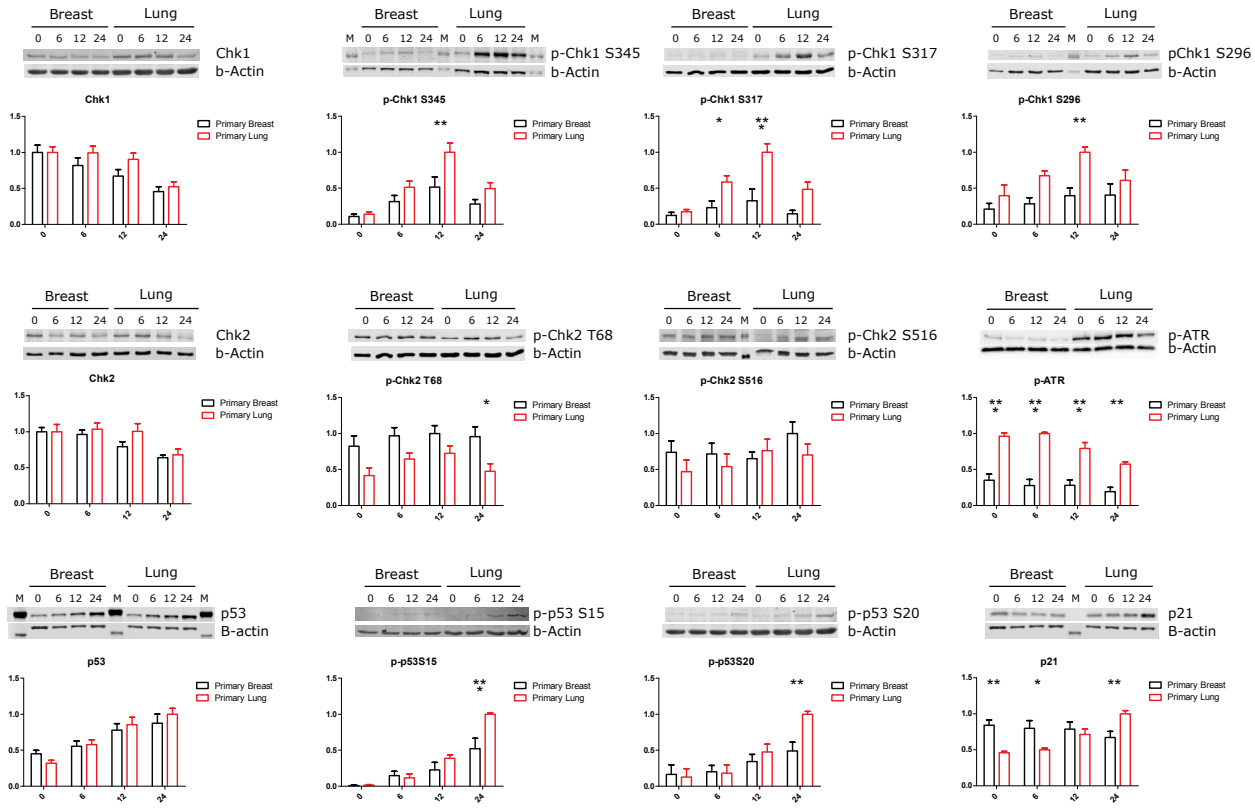

Figure S6: Time course profiles of DNA damage signaling proteins after cisplatin treatment, Related to Figure 3.

Primary breast and lung cells were treated with 20 µM or 30 µM cisplatin respectively for the indicated times. Quantitative western blot was performed for 12 (phospho) proteins (N=5-8). Error bars represent the SEM. Two way ANOVAs with Bonferroni post-hoc tests were carried out to assess if differences were significant (*=p<0.05,**=p<0.01, ***=p<0.001). Blots were incubated with antibodies of different molecular weight (or from different species) on subsequent days. Protein levels were analyzed using quantitative western blot. The protein signal was first normalized by the number cells loaded in each sample and then the level relative to the mean of maximal signal was calculated.

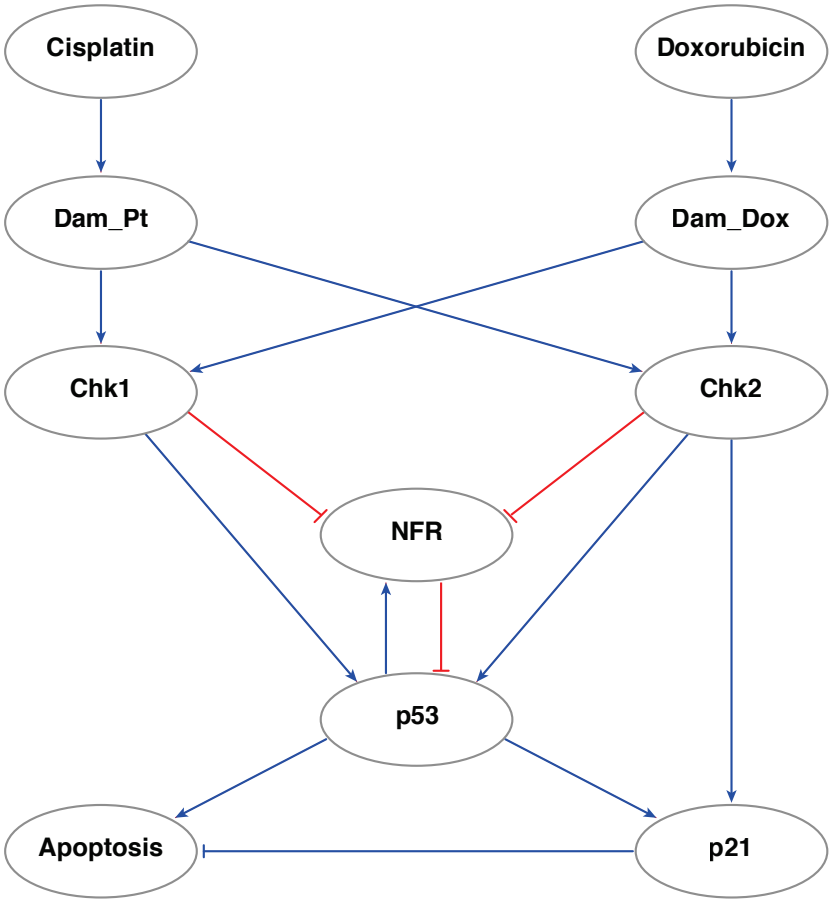

Figure S7: Model scheme showing the key regulations in the DNA damage signaling network in response to cisplatin and doxorubicin, Related to Figure 3. This diagram shows the main interactions in the model. Other reactions (e.g. protein production and degradation) are described in the supporting text in details. Blue lines indicate positive regulation and red lines indicate negative regulations.

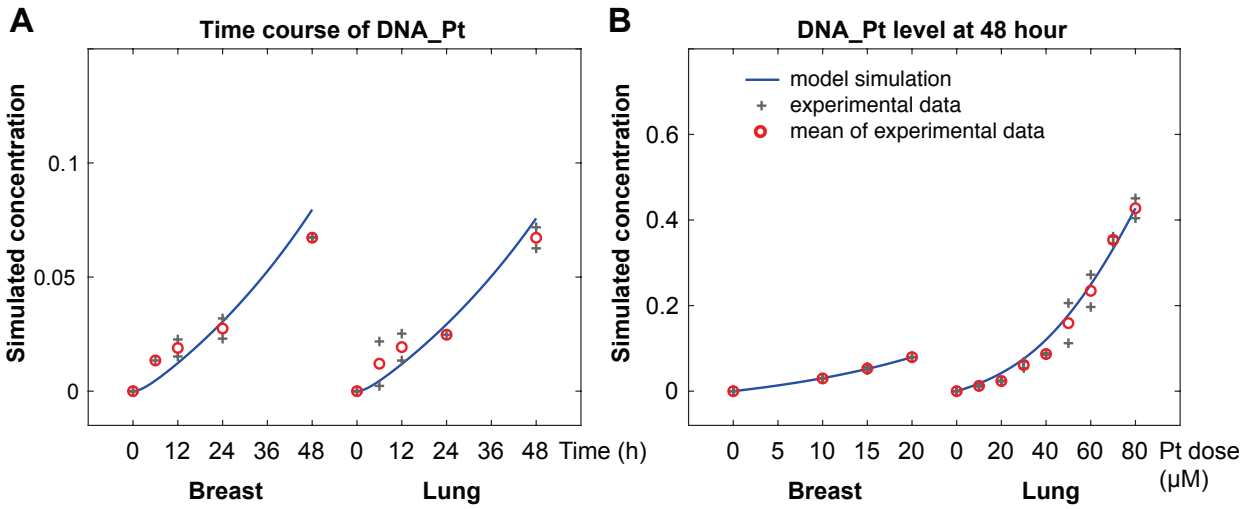

Figure S8: Comparison of model simulations to DNA bound cisplatin data, Related to Figure 3.

(A) The time course profiling of DNA bound cisplatin (Pt_DNA) in HMEPC breast (20 μM Pt) and HSAEpC lung cells (30 μM Pt). The blue line indicates the simulation results. Data from individual experiments are depicted as '+'. The average per condition is depicted as red circle.

(B) The level of Pt_DNA in breast and lung cells at 48 hour after the treatment with different doses of cisplatin. The relative levels of experimental data from 2 replicates are shown to compare with corresponding model simulations. The blue line indicates the simulation results. Data from individual experiments are depicted as '+'. The average per condition is depicted as red circle.

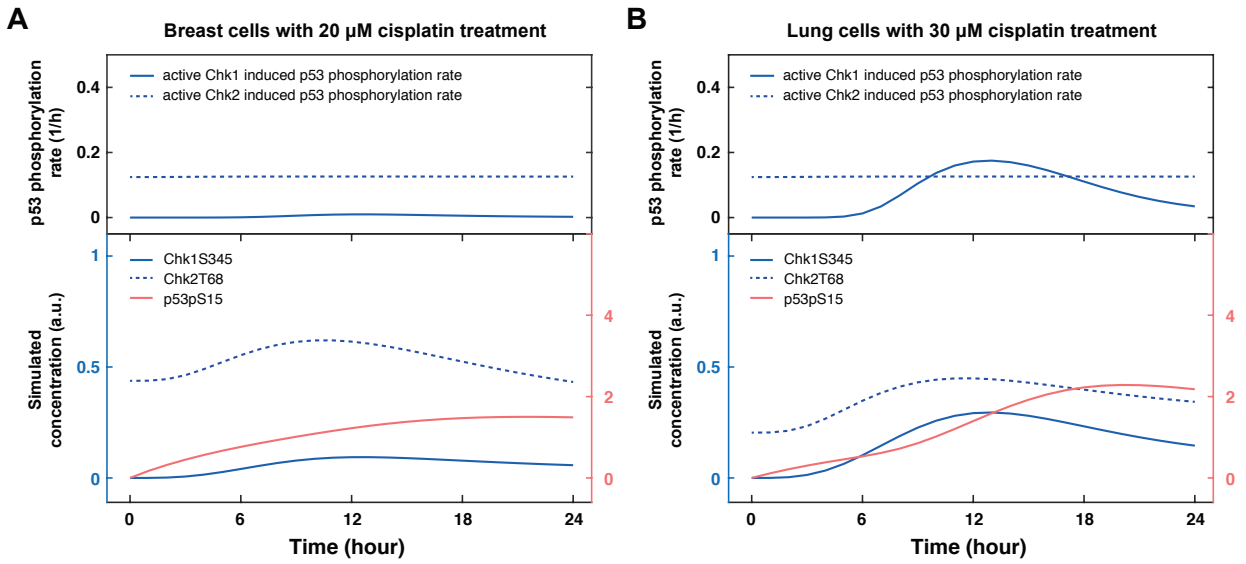

Figure S9: Model simulation analysis for the contributions of Chk1 and Chk2 activities to the dynamics of p53 phosphorylation in breast (A) and lung cells (B), Related to Figure 4. Modeling analyses show that differential Chk1 activities result in different p53 phosphorylation rates in breast and lung cells in response to cisplatin treatment.

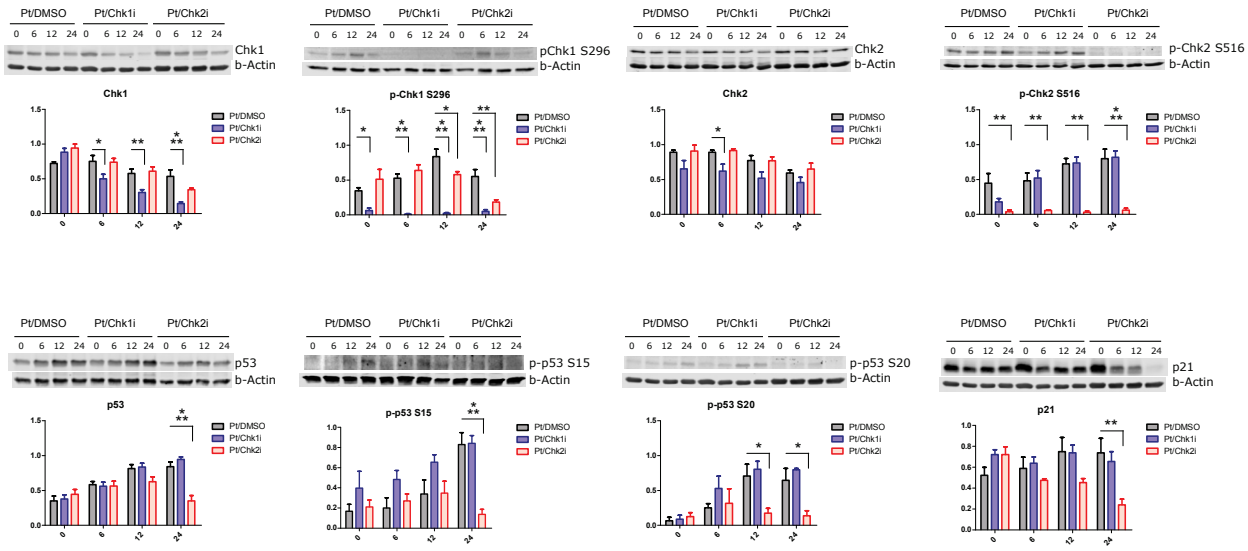

Figure S10: Effect of Chk1/Chk2 inhibitors on Chk1/Chk2 pathway activation in breast cells after cisplatin treatment, Related to Figure 4.

Primary breast cells were treated with DMSO, 1 µM PF477736 or 10 µM Chk2 inhibitor II for 1 hour, after which 20 µM cisplatin was added. Protein were isolated at indicated times, and quantitative western blot was performed (n=3-7). Error bars represent the SEM. Two way ANOVAs with Bonferroni post-hoc tests were carried out to assess if differences were significant (*=p<0.05, **=p<0.01, ***=p<0.001). Blots were incubated with antibodies of different molecular weight (or from different species) on subsequent days. The protein signal was first normalized by the number cells loaded in each sample and then the level relative to the mean of maximal signal was calculated.

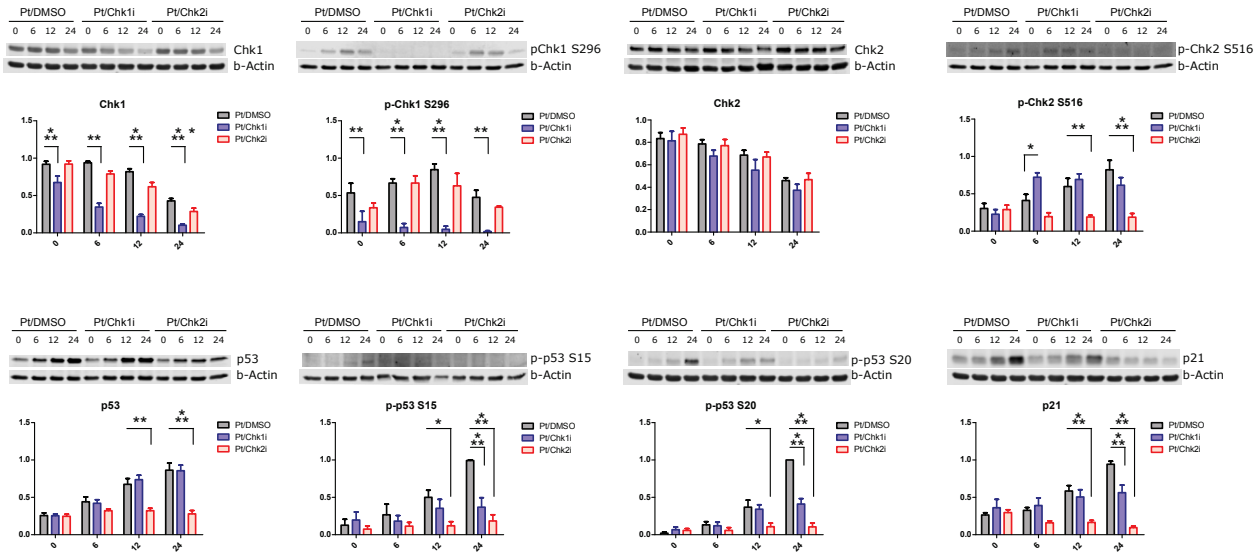

Figure S11: Effect of Chk1/Chk2 inhibitors on Chk1/Chk2 pathway activation in lung cells after cisplatin treatment, Related to Figure 4.

Primary lung cells were treated with DMSO, 1 μM PF477736 or 10 μM Chk2 inhibitor II for 1 hour, after which 30 μM cisplatin was added. Protein were isolated at indicated times, and quantitative western blot was performed (n=5-7). Error bars represent the SEM. Two way ANOVA's with Bonferroni post-hoc tests were carried out to assess if differences were significant (*=p<0.05, **=p<0.01, ***=p<0.001). Blots were incubated with antibodies of different molecular weight (or from different species) on subsequent days. The protein signal was first normalized by the number cells loaded in each sample and then the level relative to the mean of maximal signal was calculated.

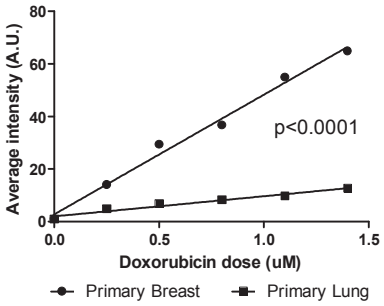

Figure S12: Intracellular doxorubicin level in primary breast and lung cells after 48 hours of doxorubicin treatment, Related to Figure 5.

Intracellular fluorescence of doxorubicin treated cells after treatment with indicated doses. After 48 hours of doxorubicin treatment, cells were trypsinized, washed with PBS and analyzed by FACS (DsRed-dtTomato filter (583/22-25). Depicted is the fold change intensity relative to untreated cells (n=3 primary breast, n=2 primary lung). Error bars represent the SD. Regression analysis was used to assess if differences in slope and intercept were significant.

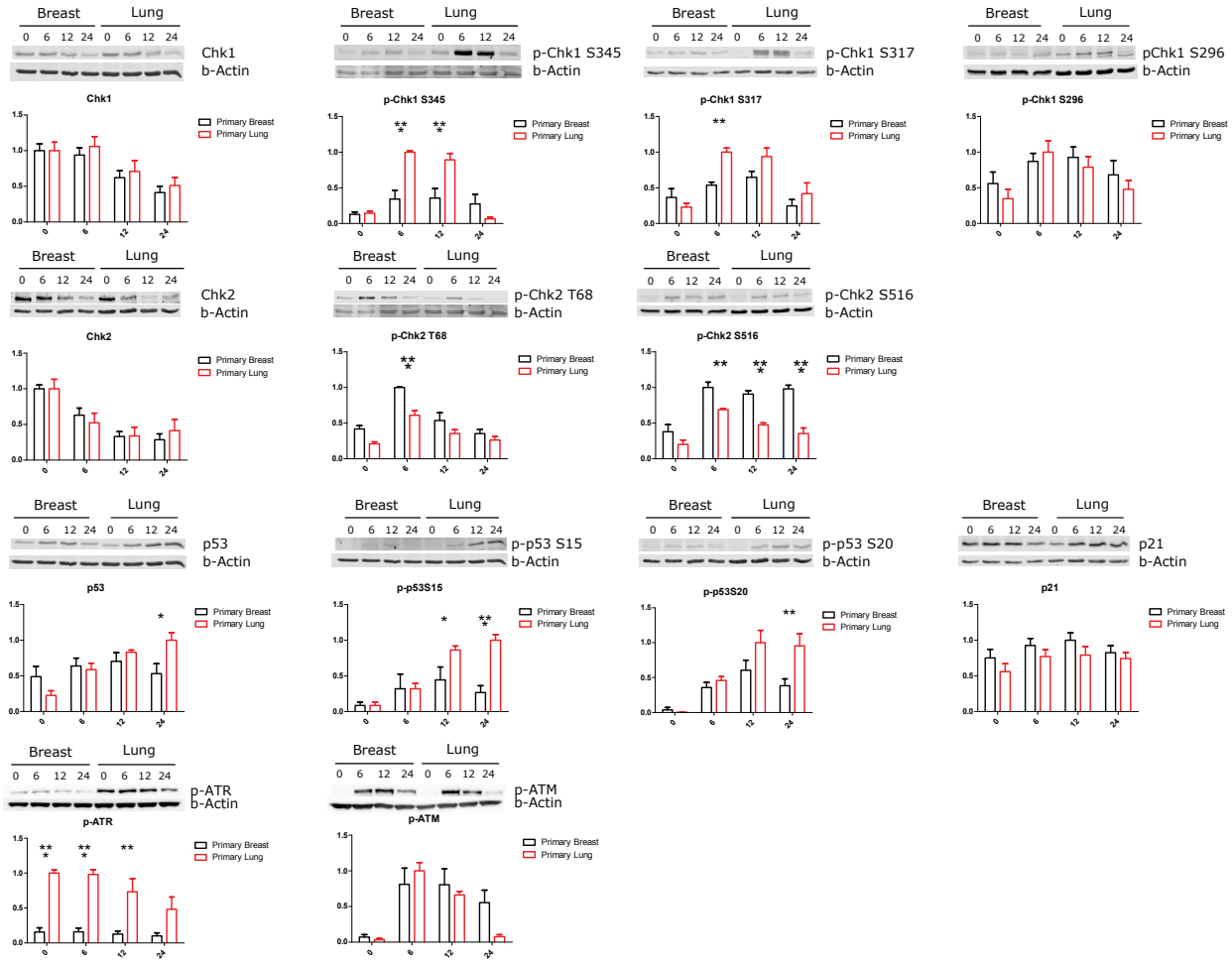

Figure S13: Activity of Chk1/Chk2 pathway after doxorubicin treatment, Related to Figure 5.

Primary breast and lung cells were treated with 0.2 µM or 1 µM doxorubicin respectively for the indicated times. Quantitative western blot was performed (N=4-6). Error bars represent the SEM. Two way ANOVA's with Bonferroni post-hoc tests were carried out to assess if differences were significant (*=$p<0.05$, **=$p<0.01$, ***=$p<0.001$). Blots were incubated with antibodies of different molecular weight (or from different species) on subsequent days. The protein signal was first normalized by the number cells loaded in each sample and then the level relative to the mean of maximal signal was calculated.

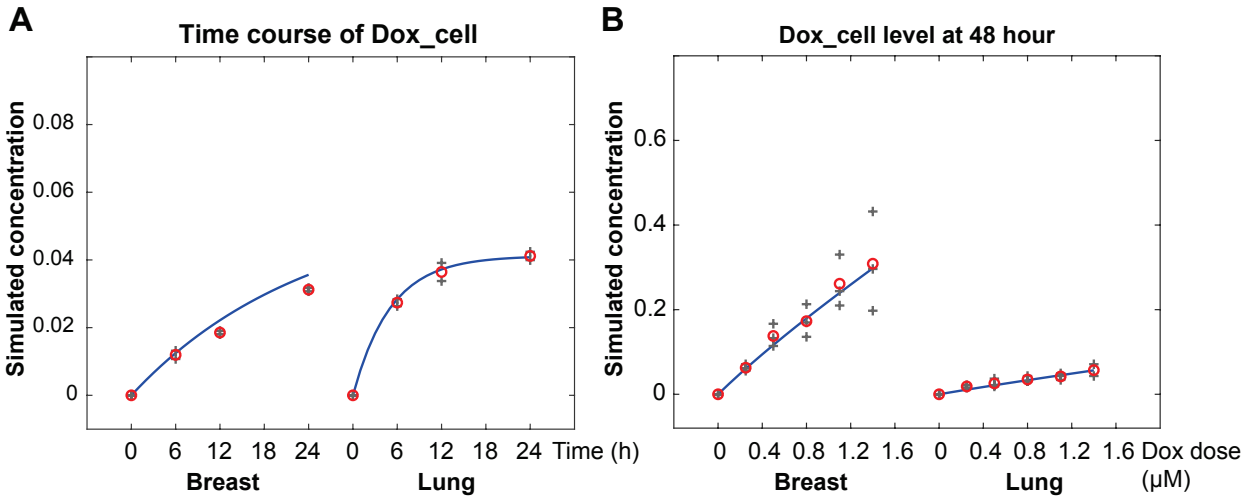

Figure S14: Comparison of model simulations to intracellular doxorubicin data, Related to Figure 5.

(A) The time course profiling of intracellular doxorubicin (Dox_cell) in breast (0.2 μM Dox) and lung cells (1 μM Dox). The blue line indicates the simulation results. Data from individual experiments are depicted as '+'. The average per condition is depicted as red circle.

(B) The level of intracellular doxorubicin (Dox_cell) in breast and lung cells at 48 hour after the treatment with different doses of doxorubicin. The relative levels of experimental data from 2-3 replicates are shown together with corresponding model simulations. The blue line indicates the simulation results. Data from individual experiments are depicted as '+'. The average per condition is depicted as red circle.

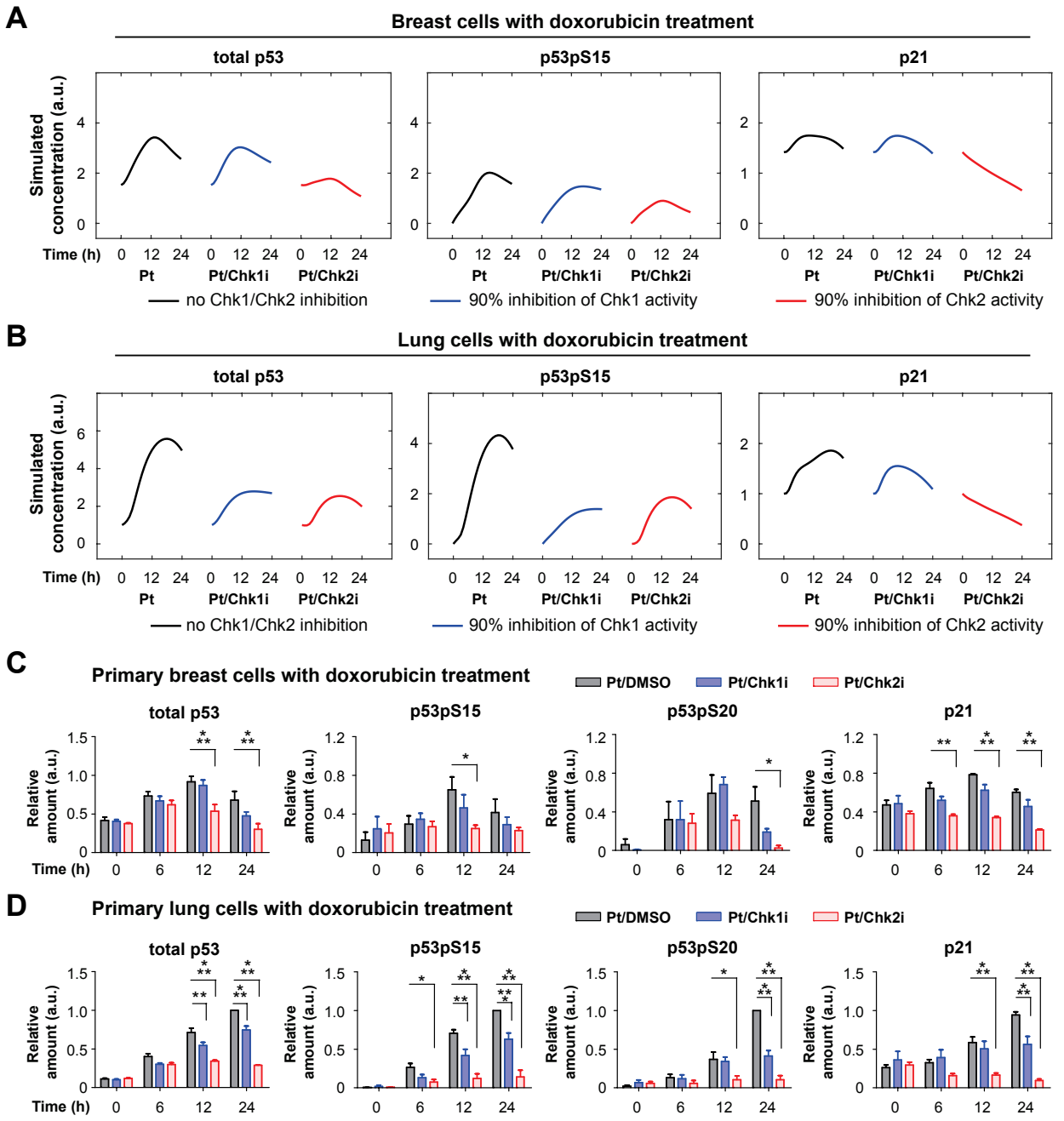

Figure S15: The effects of Chk1 and Chk2 inhibition on p53 and p21 dynamics in response to doxorubicin treatment in primary breast and lung cells, Related to Figure 5.

(A-B): Model predictions for the inhibition of Chk1 and Chk2 activities in breast (**A**) and lung cells (**B**). **(C-D):** Inhibition of Chk1 and Chk2 alter p53 and p21 dynamics. Primary breast (**C**) and lung cells **(D)** were pretreated for 1 hour with inhibitors against Chk1 (PF477736; 1 μM) and Chk2 (Inhibitor II, 10 μM), followed by doxorubicin treatment. Depicted is the average relative expression (n=3-5) for each condition normalized to the maximum value. Error bars represent the SEM. Two-way ANOVAs were used to test if a protein was differentially expressed between treatments.

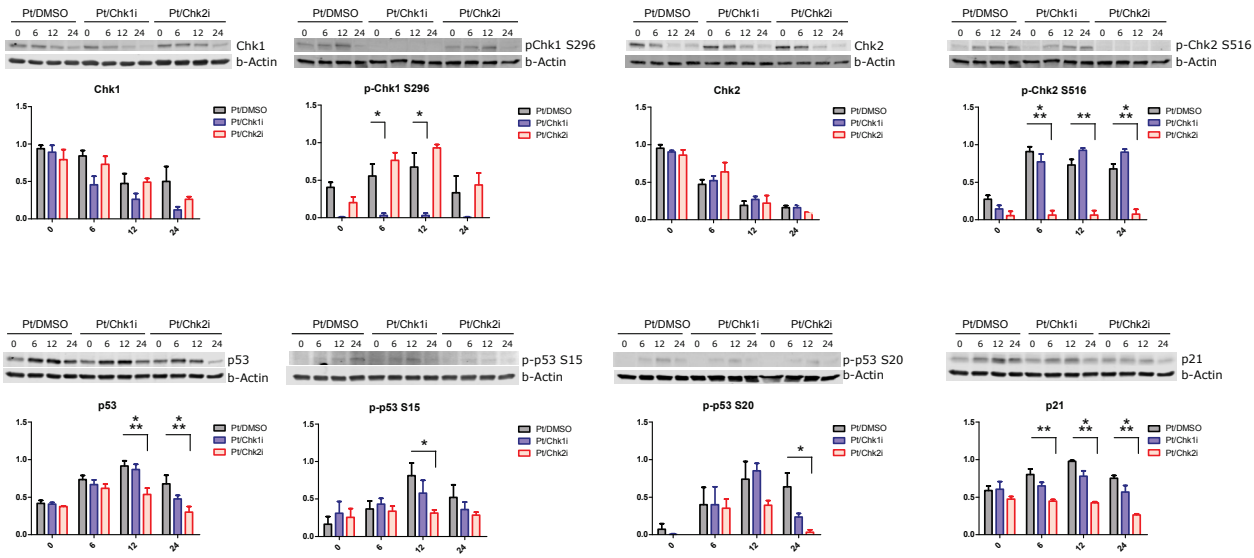

Figure S16: Activity of Chk1/Chk2 pathway in breast cells after doxorubicin treatment, Related to Figure 5.

Primary breast cells were treated with DMSO, 1 µM PF477736 or 10 µM Chk2 inhibitor II for 1 hour, after which 0.2 µM doxorubicin was added. Quantitative western blot was performed (n=3-4). Error bars represent the SEM. Two way ANOVAs with Bonferroni post-hoc tests were carried out to assess if differences were significant (*=p<0.05,**=p<0.01, ***=p<0.001). Blots were incubated with antibodies of different molecular weight (or from different species) on subsequent days. The protein signal was first normalized by the number cells loaded in each sample and then the level relative to the mean of maximal signal was calculated.

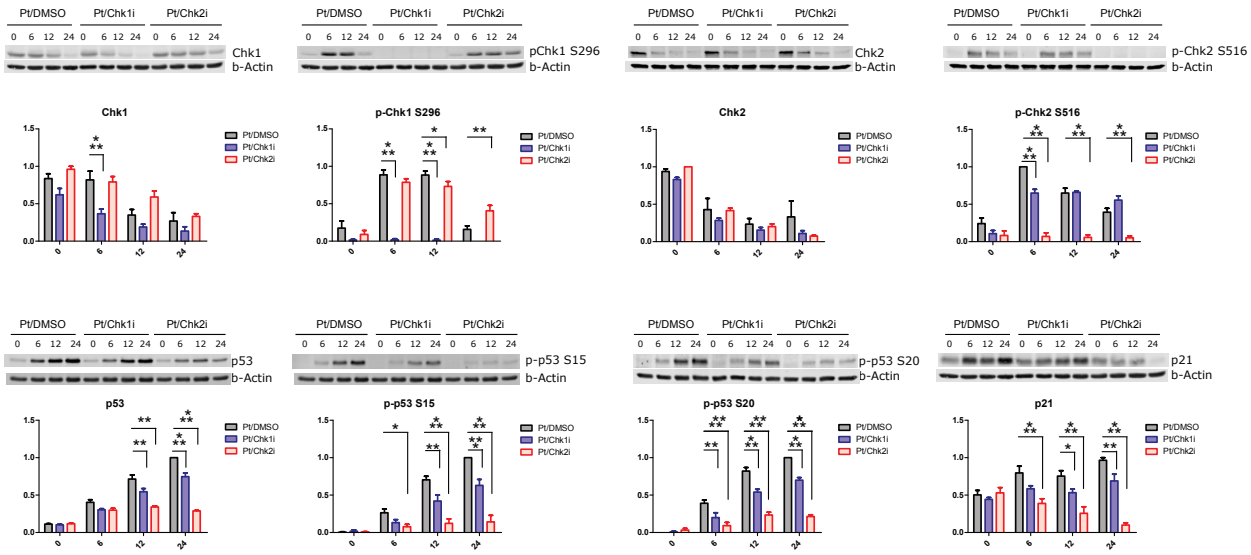

Figure S17: Activity of Chk1/Chk2 pathway in lung cells after doxorubicin treatment, Related to Figure 5.

Primary lung cells were treated with DMSO, 1 µM PF477736 or 10 µM Chk2 inhibitor II for 1 hour, after which 1 µM doxorubicin was added. Quantitative western blot was performed (n=4-5). Error bars represent the SEM. Two way ANOVA's with Bonferroni post-hoc tests were carried out to assess if differences were significant (*=p<0.05, **=p<0.01, ***=p<0.001). Blots were incubated with antibodies of different molecular weight (or from different species) on subsequent days. The protein signal was first normalized by the number cells loaded in each sample and then the level relative to the mean of maximal signal was calculated.

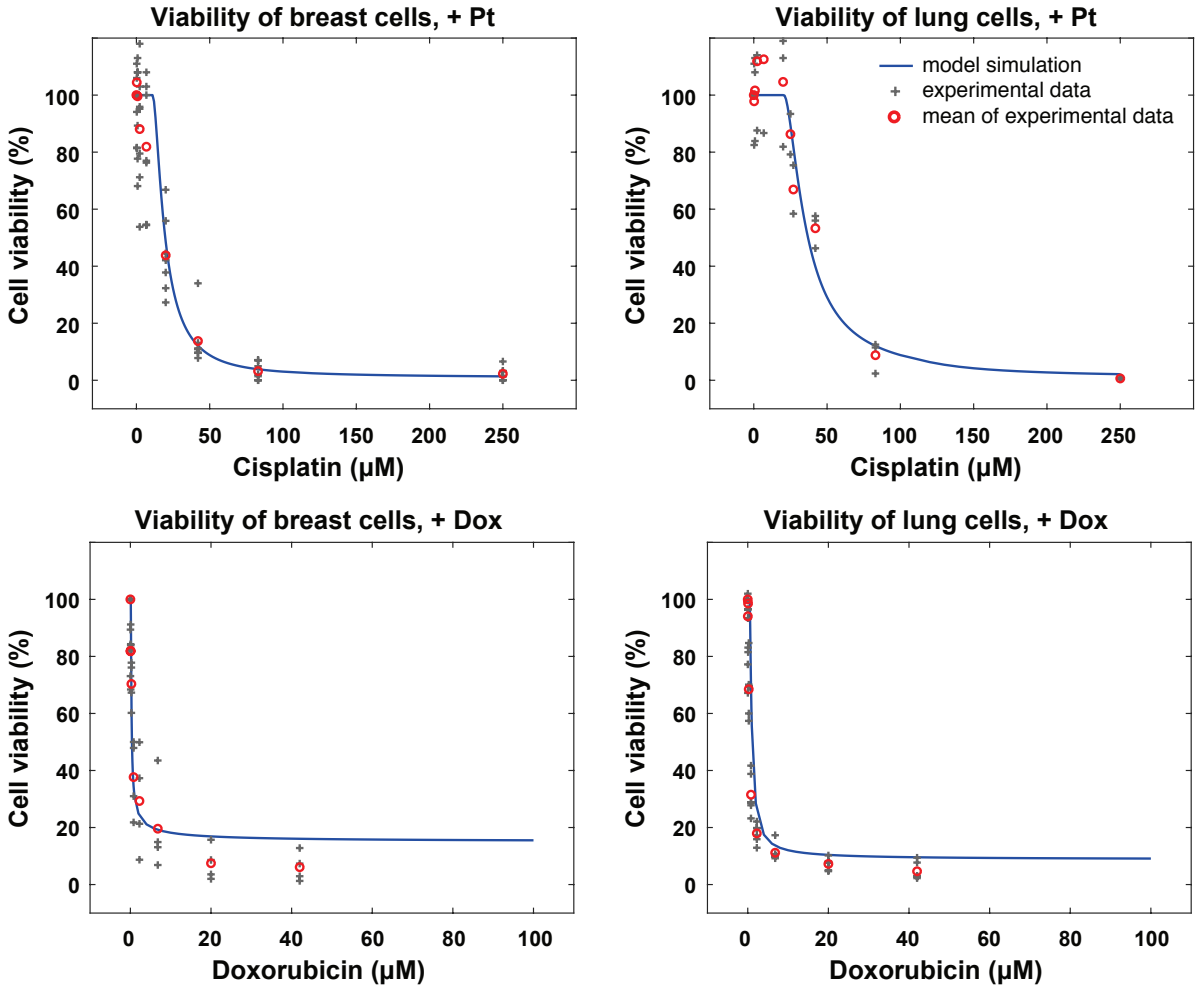

Figure S18: Model simulations for cell viability dose responses at 48 hour in breast and lung cells treated with different doses of cisplatin and doxorubicin, Related to Figure 5. Experimental data from 3-7 replicates are shown together with corresponding model simulations. The blue line indicates the simulation results. Data from individual experiments are depicted as '+'. The average per condition is depicted as red circle.

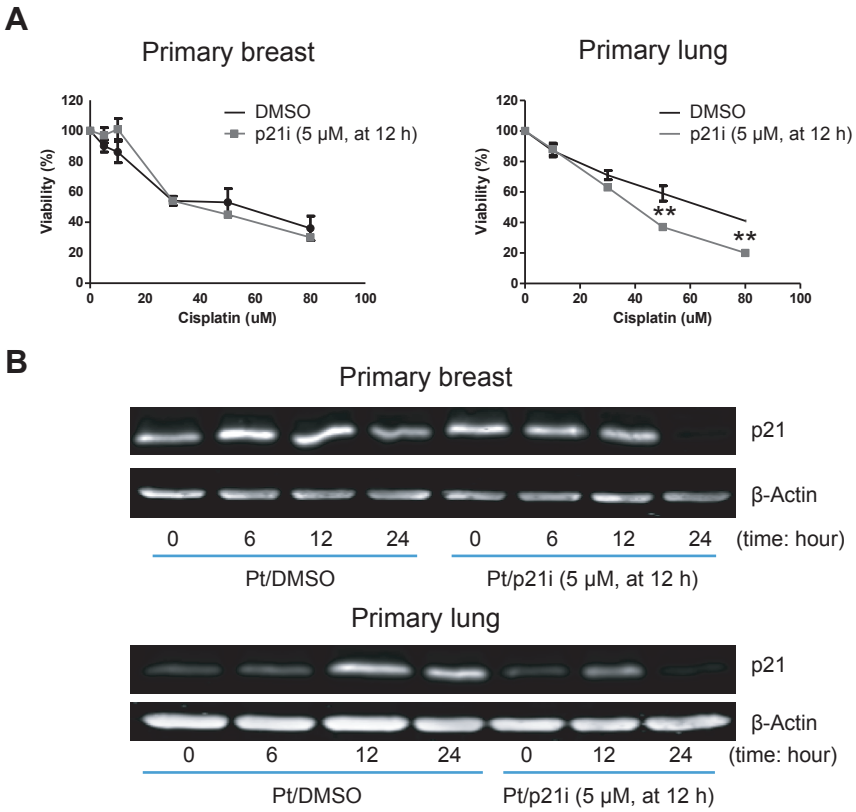

Figure S19: Effect of p21 inhibition on cisplatin response of primary breast and lung cells, Related to Figure 6.

(A) Cells were treated with cisplatin for 24 hours. After 12 hours, 5 μM UC2288 (p21 inhibitor) or an equivalent amount of DMSO was added. At 24 hour, the viability was determined. N=3, error bars represent the SD.

(B) Expression of p21 is inhibited at 24 hour in primary breast and lung cells when 5 μM UC2288 (p21 inhibitor) is added after 12 hours of cisplatin treatment.

Supplemental Tables

Table S1: Raw array data, Related to Figure 2.

Kinexus KAM-900P arrays were hybridized with control treatment (0h) and cisplatin-treated (6, 12 or 24h) breast or lung cells. Raw data shows the expression value for each antibody (present in duplicate) after scanning and Imagene spot quantification for all samples. See the corresponding Excel file.

Table S2: Array antibody validation for proteins from enriched Biocarta pathways, Related to Figure 2.

After pathway enrichment analysis of differentially expressed genes (Figure S2), antibodies recognizing key proteins from the Biocarta pathways were validated on western blot. The results from the western blot are included in the table. See the corresponding Excel file.

Table S3: Experimental conditions western blot, Related to Figure 2.

The table indicates the experimental conditions for the antibodies used for western blot. After blotting, proteins were blocked for an hour, followed by overnight first antibody incubation. See the corresponding Excel file.

Table S4: Overview of characteristics of primary cells from different donors, Related to Figure 1.

	HMEpC #1	HMEpC #2	HMEpC #3	HSAEpC #1	HSAEpC #2	HSAEpC #3
Gender	Female	Female	Female	Female	Male	Female
Age	30	41	31	48	50	65
Smoking status	Unknown	Smoker	Never Smoker	Smoker	Never smoker	Never smoker
Obtained from:	Invitrogen	Cell Systems	Promocell	Merck Millipore	Promocell	Promocell
Culture medium	Promocell Breast	Cell Systems Breast	Promocell Breast	Merck Millipore Lung, Lifeline Lung (Cell Systems)	Promocell Lung	Promocell Lung
Lot number	1462342	02904	7071104	NRG1000141	6072701.19	7110901.10
Population doubling time (H)	64	60	56	42	45	54

Note: The table contains information about the donors of the primary cells as well as the medium used to grow cells, the lot number and the population doubling time, which was determined in our experimental setting. Unless indicated otherwise HMEpC#1 (Primary breast cells #1) and HSAEpC #1 (Primary lung cells #1) were used for experiments.

Tables S5: The ratio of DNA damage response protein abundance in HMEpC breast cells compared to those in HSAEpC lung cells, Related to Figure 3 and Figure 5.

	Total Chk1	Total Chk2	Chk2pT68	Total p53	p21
Average of breast-to-lung ratio	9.97E-01	9.96E-01	2.27E+00	1.22E+00	1.53E+00
Standard error of the mean (SEM)	1.26E-01	1.33E-01	4.37E-01	1.72E-01	2.95E-01
Number of replicates	7	7	7	7	7

Note: HMEpC breast and HSAEpC lung cells were cultured under normal condition without cisplatin or doxorubicin treatment. Breast and lung cell lysates were prepared on different days (7 replicates). These samples were loaded in the same gel. Each loading sample contained proteins from an equal number of cells. We then performed immunoblotting experiments with the corresponding antibodies and estimated the relative abundance of these proteins, which was normalized by the number of cells in breast and lung cell lysate samples.

Tables S6: Initial conditions of the model, Related to Figure 3 and Figure 5.

Variable	Initial condition value in HMEpC breast cells	Initial condition value in HSAEpC lung cells
Chk1	1	1
Chk1pS345	0	0
Chk2	5.62E-01	0.796E-01
Chk2pT68	4.38E-01	2.04E-01
p53	1.53E+00	1
p53pS15	0	0
p21	1.42E+00	1
NFR	2E-01	1
Viability	1	1
Other variables	0	0

Tables S7: List of model parameters (time unit: hour), Related to Figure 3 and Figure 5.

Parameter	Description	Parameter value for cisplatin treatment		Parameter value for doxorubicin treatment	
		HMEpC breast	HSAEpC lung	HMEpC breast	HSAEpC lung
$Kimp^{Pt}_{CellType}$	Cisplatin uptake rate constant	3.37E-03	2.17E-03	--	
$K^{Pt\_cell}_{deg}$	Degradation rate constant for intracellular cisplatin (Pt_cell)	5.97E-04			
K^{Pt}_{ass}	Association rate constant for the binding of cisplatin to DNA	7.41E-03		--	
$K^{DNA\_Pt}_{deg}$	Saturating degradation rate constant for DNA-bound cisplatin (Pt_DNA)	3.87E-02		--	
J_{DNA_Pt}	Pt_DNA concentration for half-maximal Pt_DNA degradation rate	9.71E-02		--	
K^{Pt}_{dam}	Saturating rate constant for Pt_DNA induced DNA damage	4.98E-01		--	
J^{Pt}_{dam}	Pt_DNA concentration for half-maximal DNA damage rate	1.01E-02		--	
$K^{Dam\_Pt}_{rep}$	Repair rate constant for *Pt* induced DNA damage	4.35E-01		--	
$Kimp1^{Dox}_{CellType}$	Import rate constant for linear diffusion uptake of doxorubicin	--		6.55E-03	
$Kimp2^{Dox}_{CellType}$	Saturating import rate constant for carrier-mediated uptake of doxorubicin	--		1.03E-02	4.26E-03
J_{Dox}	Doxorubicin concentration for half-maximal rate of carrier-mediated uptake doxorubicin	--		1.76E+00	
$K^{Dox\_cell}_{deg,CellType}$	Saturating degradation rate constant for for intracellular doxorubicin (Dox_cell)	--		1.19E-01	5.60E-01
J_{Dox_cell}	Dox_cell concentration for half-maximal Dox_cell degradation rate	--		2.81E+00	
K^{Dox}_{dam}	Saturating rate constant for Dox_cell induced DNA damage	--		4.02E-01	
J^{Dox}_{dam}	Dox_cell concentration for half-maximal DNA damage rate	--		5.73E-02	
$K^{Dam\_Dox}_{rep}$	Repair rate constant for *Dox* induced DNA damage	--		1.92E-03	
K^{Chk1}_{prd}	Chk1 protein production rate constant	4.00E-02			
K^{Chk1}_{deg}	Chk1 protein degradation rate constant	4.00E-02			
$K^{Chk1,StressType}_{pho,CellType}$	DNA damage induced Chk1 phosphorylation rate constant	1.92E-01	3.32E-01	5.86E-01	1.59E+00
K^{Chk1}_{depho}	Chk1 dephosphorylation rate constant	1.33E-01			
$K^{Chk1p}_{deg,CellType}$	Chk1pS345 degradation rate constant	4.81E-01	7.68E-02	4.81E-01	7.68E-02
$K^{Chk1p,Pt}_{deg}$	Saturating rate constant for ubiquitin-dependent Chk1pS345 degradation after cisplatin treatment	7.57E-01		--	
J^{Chk1p}_{Pt}	Dam_Pt level for half-maximal ubiquitin-dependent Chk1pS345 degradation rate	9.35E-01		--	
$K^{Chk1p,Dox}_{deg}$	Saturating rate constant for ubiquitin-dependent Chk1pS345 degradation after doxorubicin treatment	--		6.63E-01	
J^{Chk1p}_{Dox}	Dam_Dox level for half-maximal ubiquitin-dependent Chk1pS345 degradation rate	--		4.06E+00	
K^{Chk2}_{prd}	Chk2 protein production rate constant	7.57E-02	9.03E-02	7.57E-02	9.03E-02
K^{Chk2}_{deg}	Chk2 protein degradation rate constant	7.98E-02			

$K_{deg,CellType}^{Chk2p}$	Chk2pT68 protein degradation rate constant	7.04E-02	1.44E-01	7.04E-02	1.44E-01
$K_{pho1,CellType}^{Chk2}$	Rate constant for basal Chk2 phosphorylation	6.20E-01	2.24E-01	6.20E-01	2.24E-01
$K_{pho2,CellType}^{Chk2,Pt}$	Chk2 phosphorylation rate constant induced by cisplatin	1.99E+00	1.47E+00	--	--
$K_{pho2,CellType}^{Chk2,Dox}$	Chk2 phosphorylation rate constant induced by doxorubicin	--	--	1.99E+02	2.33E+01
K_{depho}^{Chk2}	Chk2 dephosphorylation rate constant	7.27E-01			
$K_{deg}^{Chk2p,Pt}$	Saturating rate constant for ubiquitin-dependent Chk2pT68 degradation after cisplatin treatment	1.99E-01		--	
J_{Pt}^{Chk2p}	Dam_Pt level for half-maximal ubiquitin-dependent Chk2pT68 degradation rate	7.38E-01		--	
$K_{deg}^{Chk2p,Dox}$	Saturating rate constant for ubiquitin-dependent Chk2pT68 degradation after doxorubicin treatment	--		1.87E-01	
J_{Dox}^{Chk2p}	Dam_Dox level for half-maximal ubiquitin-dependent Chk2pT68 degradation rate	--		1.70E-01	
$K_{prd,CellType}^{p53}$	p53 protein production rate constant	1.53E+00	3.91E+00	1.53E+00	3.91E+00
K_{deg1}^{p53}	NFR independent p53 degradation rate constant	2.74E-01			
K_{deg2}^{p53}	NFR dependent p53 degradation rate constant	3.64E+00			
K_{deg1}^{p53p}	NFR independent p53pS15 degradation rate constant	5.22E-02			
K_{deg2}^{p53p}	NFR dependent p53pS15 degradation rate constant	1.01E-02			
K_{pho1}^{p53}	Saturating rate constant for active Chk1 induced p53 phosphorylation	3.96E-01			
J_{1}^{p53}	Chk1pS345 concentration for half-maximal p53 phosphorylation rate	3.19E-01			
K_{pho2}^{p53}	Saturating rate constant for active Chk2 induced p53 phosphorylation	1.26E-01			
J_{2}^{p53}	Chk2pT68 concentration for half-maximal p53 phosphorylation rate	5.00E-02			
K_{depho}^{p53}	p53 dephosphorylation rate constant	6.25E-02			
$K_{prd1,CellType}^{NFR}$	p53-independent NFR production rate constant	2.06E-02	4.87E-02	2.06E-02	4.87E-02
K_{prd2}^{NFR}	Saturating rate constant for p53-dependent NFR production	2.50E-02			
J_{p53p}^{NFR}	p53pS15 concentration for half-maximal p53-dependent NFR production	1.58E+00			
K_{deg1}^{NFR}	NFR degradation rate constant	1.38E-03			
K_{deg2}^{NFR}	Chk1pS345 dependent NFR degradation rate constant	1.76E-02			
K_{deg3}^{NFR}	Chk2pT68 dependent NFR degradation rate constant	2.32E-01			
K_{prd1}^{p21}	p21 basal production rate constant	1.91E-02			
$K_{prd2,CellType}^{p21}$	Rate constant for Chk2pT68 dependent p21 production	1.30E-01	2.59E-01	1.30E-01	2.59E-01
$K_{prd3}^{p21,Pt}$	Saturating rate constant for p53pS15 dependent p21 production, with cisplatin	6.73E+00		--	
$K_{prd3}^{p21,Dox}$	Saturating rate constant for p53pS15 dependent p21 production, with doxorubicin	--		6.37E-01	
J_{p53p}^{p21}	p53pS15 concentration for half-maximal p53-dependent p21 production	3.92+00			
$K_{deg}^{p21,CellType}$	p21 basal degradation rate constant	5.35E-02	7.21E-02	5.35E-02	7.21E-02

$K_{deg}^{p21,Pt}$	Saturating rate constant for proteasomal degradation of p21 after cisplatin treatment	3.25E+00		--	
J_{Pt}^{p21}	Dam_Pt level for half-maximal proteasomal degradation rate of p21	2.11E+00		--	
$K_{deg}^{p21,Dox}$	Saturating rate constant for proteasomal degradation of p21 after doxorubicin treatment	--		1.20E+00	
J_{Dox}^{p21}	Dam_Dox level for half-maximal proteasomal degradation rate of p21	--		8.27E+00	
$K_{birth}^{CellType}$	Cell birth rate constant (characterized by doubling time)	1.08E-02	1.65E-02	1.08E-02	1.65E-02
$K_{death}^{StressType}$	p53-threshold dependent cell death (apoptosis) rate constant	9.21E-02		3.30E-02	
μ	Scaling factor of p21-dependent apoptosis threshold (similar to the friction coefficient)	3.62E+00			
τ	Time delay for active p53 regulated protein production	2			

Transparent Methods

Cell culture and reagents

Human Mammary Epithelial progenitor Cells (HMEpC) and Small Airway Epithelial progenitor Cells (HSAEpC) were obtained from Promocell, Thermofisher Scientific, Cell technologies and Merck Millipore (Table S4). HMEpC cells can give rise to both luminal and basal epithelial cells, and as such are related to the predecessors of luminal- and basal-type breast cancer (Dimri et al., 2005). HSAEpC cells are isolated from the distal portion of the respiratory tract and comprise cells from bronchioli and alveoli. These cells are the closest culturable representatives of predecessors of lung adenocarcinomas. All primary cell cultures retain their characteristics for 16 population doublings. Cells were cultured in the company's culture media, grown until population doubling 5, then frozen and aliquoted. For every experiment, a cryovial was thawed, and the experiment was performed in population doubling 10-12 (van Jaarsveld et al., 2014). Key observations were repeated with cells from different donors.

Cisplatin (1 mg/mL Platosin solution) and doxorubicin (2 mg/mL solution) were obtained from Accord and Teva Germany, respectively. Inhibitors were obtained from Adipogen (p38 MAPK inhibitor SB203580), Cayman chemicals (JNK inhibitor SP-600125, Chk2 inhibitor II, ATR inhibitor VE822), Cell Signaling Technologies (MEK inhibitor U0126, PI3K inhibitor LY294002), Merck Millipore (p21 inhibitor UC2288) and Sigma-Aldrich (Chk1 inhibitor PF-477736).

MTT assay

At the indicated times, 20 μL (96-wells plates) or 50 μL (24-wells plates) of 5 mg/mL MTT in PBS was added to the plates, and plates were incubated at 37 ^{0}C for 4 hours. Then, the medium was discarded and 200 μL (96-wells plates) or 500 μL (24-wells plates) DMSO was added. The absorbance was measured at 560 nm. For the cisplatin dose response experiments with inhibitors, cell viability data were normalized to the 0 μM cisplatin treatment (in the case of DMSO: DMSO + 0 μM cisplatin; in the case of inhibitor: inhibitor + 0 μM cisplatin).

Protein array

Cells were washed 2x in PBS and lysed in Kinexus lysis buffer (20 mM MOPS, pH 7, 2 mM EGTA, 5 mM EDTA, 30 mM NaF, 60 mM beta-glycerophosphate, pH 7.2, 20 mM sodium pyrophosphate, 1 mM Na3VO4, 1% Triton X-100, 1 mM DTT, 1 mM PMSF and Complete protease inhibitors (Roche) at a concentration >2 μg/μL). The lysates were sheared with a syringe/26G needle, and spun down at 16.000 x g for 30 min at 4 ^{0}C. The supernatants were stored at -80 ^{0}C, and shipped on dry ice to the Kinexus Bioinformatics Corporation (Vancouver, Canada), where the lysates were processed and profiled on a KAM-900P protein array (contains

265 pan-specific and 613 phospho-specific antibodies). On each array, a control sample (0h) was cohybridized with a cisplatin-treated sample (6, 12 or 24h) (Table S1). The raw data was normalized using quantile normalization, and obvious outliers were removed. Z-score ratios were calculated for (i) the expression changes of treated vs untreated samples for both HMEpC and HSAEpC (Z score time point – Z score 0h / stdev Z scores over all time points) and (ii) the differential expression of HMEpC vs. HSAEpC for each time point (Z score HMEpC – Z score HSAEpC/ stdev HMEpC-HSAEpC Z-scores over all time points). Candidates that had a Z-score ratio over 1.2 and a fold change over 1.5 were considered differentially expressed. Pathway analysis was performed using DAVID pathway analysis tool (version 6.7) (Dennis et al., 2003; Huang da et al., 2009) (Table S2).

Western blot

Proteins were isolated with RIPA protein lysis buffer (Cell Signaling Technology), and 20 μg of protein was analyzed on SDS-PAGE gel (~94000 HMEpC cells, ~115000 HSAEpC cells). Proteins with a MW under 200 kDa were analyzed on 12% Tris-Glycine gels, which were transferred onto a 0.45 μM nitrocellulose membrane by dry blotting. Proteins with a MW above 200 kDa were analyzed on Criterion 3-8% Tris-Acetate gels (BioRad), which were run with Tricine Running buffer (BioRad) and were transferred onto a 0.2 μM nitrocellulose membrane by wet blotting. For an overview of detection of specific proteins, see Table S3.

Platinum measurements

DNA was isolated at the indicated time points, and stored at -20 until analysis. To measure platinum bound to the DNA, 1% HNO3 was added to the DNA. The platinum content in DNA lysates (peak at 265.9 nm) was determined using Atomic Absorption Spectrometry. (Burger et al., 2010)

Immunofluorescence

Cells were plated on cover slips in 24-wells plates (HSAEpC: 40,000 cells/well; HMEpC 20,000 cells/well). At indicated times, samples were washed 1x with PBS, followed by 10 min incubation in 4% Paraformaldehyde solution/PBS pH 7.2. Afterwards, coverslips were washed 2x with PBS, followed by blocking in 3% BSA/PBS-Tween-20 for 30 min. Overnight incubation with primary antibody (yH2AX; 1:500 in blocking buffer; Abcam #Ab22551) took place at 4 ^{0}C. Afterwards, samples were washed 3x with PBST, followed by secondary antibody incubation (Goat-anti-Mouse Alexa 555; Cell Signaling #4409S; 1:600 in PBST) for 1 hour. After washing 3x in PBST and 1x in PBS, samples were mounted in Prolong Gold + DAPI (Cell Signaling, 8961S), and after 24 hours of drying, sealed with nail polish.

FACS

To determine the intracellular fluorescence of doxorubicin, cells were trypsinized, washed 2x with PBS, after which they were kept on ice and analyzed by FACS within one hour (dose response curve) or fixated in 2% PFA/PBS for 30 min at 4 ^{0}C, washed 2x with ice-cold PBS, stored at 4 ^{0}C and measured within 4 days (time course experiment). The median fluorescence intensity of doxorubicin was measured using the 561 laser and DsRed-dt Tomato filter (583/22-25).

Statistical analysis

Two-way ANOVA was used to determine whether cell type and/or treatment time had a significant effect in Figures 1D, 2D, 3A, 4C-D, 5B. In case of a positive result, Bonferroni post-hoc tests were conducted to compare the level for each cell type for each time point. To compare the difference in IC_{50} value between primary breast and lung cells (Figure 1B) a t-test was carried out. Linear regression analysis was performed to compare slope and intercept of breast and lung curves in Figure 1E, 5A. All tests are two-tailed. Significant differences are indicated in the figures.

Mathematical Modeling

The DNA damage response network was modeled with a system of ordinary differential equations (ODEs). The optimization of model parameters was performed with the parallel parameter estimation tool SBML-PET-MPI (Zi, 2011). Model simulations were performed with a customized tool SBML-SAT (Zi et al., 2008) in Matlab. Additional details are provided in the Supplemental Text.

Supplemental Text

Mathematical modeling of the DNA damage response to cisplatin and doxorubicin

We developed an integrated mathematical model for the DNA damage response to cisplatin (Pt) and doxorubicin (Dox) treatments based our data and previous studies (Barr et al., 2017; Batchelor et al., 2011; Batchelor et al., 2008; Ma et al., 2005; Stewart-Ornstein and Lahav, 2017; Zhang et al., 2011). In this new model, we considered the following interaction modules: (1) the module for Pt uptake and Pt induced DNA damage (Dam_Pt) to account for the upstream signaling processes of Pt treatment; (2) the module for Dox uptake and Dox induced DNA damage (Dam_Dox) to account for the upstream signaling processes of Dox treatment; (3) the regulations of p21 by p53 and Chk2 activities; (4) a dynamic p53 threshold mechanism for the trigger of apoptosis to account for the cell viability response. In the models for human primary breast (HMEpC) and lung (HSAEpC) cells, we used the same model structure and the same reaction kinetics. Most parameter values are the same for the models of breast and lung cells, except that some kinetic parameters were set with different values to distinguish the observed different cellular uptake rates of cisplatin and doxorubicin, differential activation and degradation of proteins, and others specified in Table S7. The scheme of the model is presented in Figure S7. The dynamics of the involved signaling molecules are described as a set of ordinary differential equations (ODEs). The modeling rationale and reaction kinetics for different signaling steps are described below.

Modeling the cellular uptake dynamics of cisplatin and doxorubicin

We used a simple kinetic model to describe the cellular uptake dynamics of cisplatin based on a model developed by Kareh & Secomby (El-Kareh and Secomb, 2003). The model includes the kinetics of intracellular cisplatin (*Pt_cell*) and DNA-bound cisplatin (*Pt_DNA*) with the following differential equations:

$$\frac{d[Pt\_cell]}{dt} = K_{imp,CellType}^{Pt}[Pt] - K_{ass}^{Pt}[Pt\_cell] - K_{deg}^{Pt\_cell}[Pt\_cell] \quad \text{E1}$$

$$\frac{d[Pt\_DNA]}{dt} = K_{ass}^{Pt}[Pt\_cell] - K_{deg}^{DNA\_Pt}\frac{[Pt\_DNA]}{J_{DNA\_Pt} + [Pt\_DNA]} \quad \text{E2}$$

If we take a 6-well plate experimental setup with 2×10^5 cells in 4 mL medium and assume the estimated human epithelial cell size is ~2×10^{-12} L, the ratio of medium to cell volume will be about 10000. Therefore, only a very small fraction of cisplatin will be transported into cells. Indeed, Centerwall *et al.* has shown that the concentration of cisplatin in the medium remains almost constant (Centerwall et al., 2006). In this model, we assume the concentration of cisplatin ([*Pt*]) in the medium is constant over time.

We used two different parameters $K_{imp,B}^{Pt}$ and $K_{imp,L}^{Pt}$ to specify the different cisplatin update rates observed in HMEpC breast and HSAEpC lung cells (Figure S1C). The kinetic parameters in equations E1-E2 were optimized with the experimental data sets for *Pt_DNA* in both breast and lung cells. As is shown in Figure S8, this simple model can fit different kinds of *Pt_DNA* data very well.

Previous studies have shown that doxorubicin may enter cells with a combination of linear diffusive and carrier-mediated uptake mechanisms (El-Kareh and Secomb, 2005; Nagasawa et al., 1996). We modeled the cellular dynamics of intracellular doxorubicin (*Dox_cell*) with the following differential equation based on the cellular pharmacokinetic model proposed by EI-Kareh & Secomb (El-Kareh and Secomb, 2005):

$$\frac{d[Dox\_cell]}{dt} = K_{imp1}^{Dox}[Dox] + \frac{K_{imp2,CellType}^{Dox}[Dox]}{J_{Dox} + [Dox]} - \frac{K_{deg}^{Dox\_cell}[Dox\_cell]}{J_{Dox\_cell} + [Dox\_cell]} \quad \text{E3}$$

The concentration of doxorubicin in the medium ([*Dox*]) is assumed to be constant over time, which is the dose of doxorubicin applied to the cells. The kinetic parameters in equations E3 were optimized with the experimental data for intracellular doxorubicin (*Dox_cell*) dynamics in breast and lung cells. As shown in Figure S14, this model can reproduce different kinds of *Dox_cell* data very well.

Modeling DNA damage and DNA repair induced by cisplatin and doxorubicin

Cisplatin induced DNA damage (*Dam_Pt*) is modeled by taking into account the DNA damage triggered by DNA-bound cisplatin (*Pt_DNA*) and the repair of DNA-Pt lesions.

$$\frac{d[Dam\_Pt]}{dt} = K_{dam}^{Pt}\frac{[DNA\_Pt]}{J_{dam}^{Pt} + [DNA\_Pt]} - K_{rep}^{Dam\_Pt}[Dam\_Pt] \quad \text{E4}$$

Similarly, doxorubicin induced DNA damage (*Dam_Dox*) is modeled with a forward reaction triggered by intracellular doxorubicin (*Dox_cell*) and a backward reaction for DNA repair.

$$\frac{d[Dam\_Dox]}{dt} = K_{dam}^{Dox}\frac{[Dox\_cell]}{J_{dam}^{Dox} + [Dox\_cell]} - K_{rep}^{Dam\_Dox}[Dam\_Dox] \quad \text{E5}$$

Modeling the dynamics of Chk1 and Chk2

Previous work has shown that after Chk1 and Chk2 activation, Chk1 and Chk2 are down regulated by DNA damage stresses involving ubiquitination (Bohgaki et al., 2013; Garcia-Limones et al., 2016; Kass et al., 2007; Zhang et al., 2009; Zhang et al., 2005). Therefore, we used the following differential equations to model the dynamics of Chk1, Chk1pS345, Chk2 and Chk2T68.

$$\begin{aligned}\frac{d[Chk1]}{dt} = {} & K_{prd}^{Chk1} - K_{deg}^{Chk1}[Chk1] \\ & - H(Pt)K_{pho,CellType}^{Chk1,Pt}[Dam\_Pt][Chk1] \\ & - H(Dox)K_{pho,CellType}^{Chk1,Dox}[Dam\_Dox][Chk1] \\ & + K_{depho}^{Chk1}[Chk1pS345]\end{aligned} \quad \text{E6}$$

$$\begin{aligned}\frac{d[Chk1pS345]}{dt} &= H(Pt)K_{pho,CellType}^{Chk1,Pt}[Dam\_Pt][Chk1] \\ &\quad +H(Dox)K_{pho,CellType}^{Chk1,Dox}[Dam\_Dox][Chk1] \\ &-K_{depho}^{Chk1}[Chk1pS345] - K_{deg,CellType}^{Chk1p}[Chk1pS345] \\ &-K_{deg}^{Chk1p,Pt}\frac{[Dam\_Pt]^3}{(J_{Pt}^{Chk1p})^3 + [Dam\_Pt]^3}[Chk1pS345] \\ &-K_{deg}^{Chk1p,Dox}\frac{[Dam\_Dox]^3}{(J_{Dox}^{Chk1p})^3 + [Dam\_Dox]^3}[Chk1pS345]\end{aligned} \quad \text{E7}$$

The $H(x)$ function is a Heaviside generalized function ($H(x) = 1, if\ x > 0;\ H(x) = 0, if\ x \leq 0$), which helps the model to specify different reaction kinetics for cisplatin and doxorubicin treatments, meaning:

$$H(Pt) = 1, for\ cisplatin\ treatment\ (Pt > 0); Otherwise, H(Pt) = 0\ (Pt \leq 0); \quad \text{E8}$$

$$H(Dox) = 1, for\ doxorubicin\ treatment\ (Dox > 0); Otherwise, H(Dox) = 0\ (Dox \leq 0); \quad \text{E9}$$

We observed that there is obvious basal phosphorylation of Chk2 at the T68 site in both breast and lung cells even without cisplatin or doxorubicin treatment. Therefore, we considered the basal Chk2pT68 level, which resulted in the following equations:

$$\begin{aligned}\frac{d[Chk2]}{dt} &= K_{prd,CellType}^{Chk2} - K_{deg}^{Chk2}[Chk2] - K_{pho1,CellType}^{Chk2} + K_{depho}^{Chk2}[Chk2pT68] \\ &\quad -H(Pt)K_{pho2,CellType}^{Chk2,Pt}[Dam\_Pt][Chk2] \\ &\quad -H(Dox)K_{pho2,CellType}^{Chk2,Dox}[Dam\_Dox][Chk2]\end{aligned} \quad \text{E10}$$

$$\begin{aligned}\frac{d[Chk2pT68]}{dt} &= K_{pho1,CellType}^{Chk2}[Chk2] \\ &\quad +H(Pt)K_{pho2,CellType}^{Chk2,Pt}[Dam\_Pt][Chk2] \\ &\quad +H(Dox)H(Dox)K_{pho2,CellType}^{Chk2,Dox}[Dam\_Dox][Chk2] \\ &\quad -K_{depho}^{Chk2}[Chk2pT68] - K_{deg,CellType}^{Chk2p}[Chk2pT68] \\ &\quad -K_{deg}^{Chk2p,Pt}\frac{[Dam\_Pt]^3}{(J_{Pt}^{Chk2p})^3 + [Dam\_Pt]^3}[Chk2pT68] \\ &\quad -K_{deg}^{Chk2p,Dox}\frac{[Dam\_Dox]^3}{(J_{Dox}^{Chk2p})^3 + [Dam\_Dox]^3}[Chk2pT68]\end{aligned} \quad \text{E11}$$

Modeling the dynamics of p53

In the model, we used a negative feedback regulator variable (NFR) to implicitly represent the lumped effect of negative feedback regulations (e.g. Mdm2/MdmX and others) on p53 (Love and Grossman, 2012). The variable p53pS15 represents the active form of p53. We also considered the regulation of NFR by upstream Chk1pS345 and Chk2pT68 signaling, which can phosphorylate MDMX (Chen et al., 2005; Jin et al., 2006; LeBron et al., 2006), resembling the effect of ATR and ATM activity on MDM2 in Batchelor-MSB-2011 model. Please note however, that these negative regulators have different

mode of actions and that their exact role and contribution needs to be addressed in further studies. We used the following equation to describe the dynamics of p53 proteins:

$$\frac{d[p53]}{dt} = K_{prd}^{p53} - K_{deg1}^{p53}[p53] - K_{deg2}^{p53}[NFR][p53] + K_{depho}^{p53}[p53pS15] - \left(\frac{K_{pho1}^{p53}[Chk1pS345]^3}{(J_1^{p53p})^3 + [Chk1pS345]^3} + \frac{K_{pho2}^{p53}[Chk2pT68]^3}{(J_2^{p53p})^3 + [Chk2pT68]^3}\right) \quad \text{E12}$$

$$\frac{d[p53pS15]}{dt} = \frac{K_{pho1}^{p53}[Chk1pS345]^3}{(J_1^{p53p})^3 + [Chk1pS345]^3} + \frac{K_{pho2}^{p53}[Chk2pT68]^3}{(J_2^{p53p})^3 + [Chk2pT68]^3} - K_{deg1}^{p53p}[p53pS15] - K_{deg2}^{p53p}[NFR][p53pS15] - K_{depho}^{p53}[p53pS15] \quad \text{E13}$$

$$\frac{d[NFR]}{dt} = K_{prd1}^{NFR,CellType} - K_{deg1}^{NFR}[NFR] - K_{deg2}^{NFR}[Chk1pS345] - K_{deg3}^{NFR}[Chk2pT68] + K_{prd2}^{NFR}\frac{[p53pS15(t-\tau)]^3}{(J_{p53p}^{NFR})^3 + [p53pS15(t-\tau)]^3} \quad \text{E14}$$

The variable $p53pS15(t-\tau)$ represents the delayed accumulation of p53pS15 with time τ. The delay of p53pS15 was modeled with a series of intermediate states using the linear chain tricks.

$$\frac{d[z1]}{dt} = \frac{2\,([p53pS15] - [z1])}{\tau} \quad \text{E15}$$

$$\frac{d[z2]}{dt} = \frac{2\,([z1] - [z2])}{\tau} \quad \text{E16}$$

After combining equations E15-E16, the $p53pS15(t-\tau)$ delay variable can be replaced by the $z2$ variable. We set the delay time τ = 2 hours, the same value used in a recent p53 kinetic model reported by Stewart-Ornstein & Lahav (Stewart-Ornstein and Lahav, 2017).

Modeling the dynamics of p21

Previous reports have shown that Chk2 positively regulates p21 expression in p53-dependent and p53-independent ways (Aliouat-Denis et al., 2005; Loughery et al., 2014; Macleod et al., 1995), although the p53-independent effects are less well documented and mainly based on overexpression studies. In addition, p21 is also down-regulated through proteasomal degradation after DNA damage stress stimulations (Abbas and Dutta, 2009; Bloom et al., 2003; Jin et al., 2003). Therefore, the dynamic of p21 protein is described with the following differential equation:

$$\frac{d[p21]}{dt} = K_{prd1}^{p21} + \left(K_{prd2,CellType}^{p21} + (H(Pt)K_{prd3}^{p21,Pt} + H(Dox)K_{prd3}^{p21,Dox})\frac{[z2]^3}{(J_{p53p}^{p21})^3 + [z2]^3}\right)[Chk2pT68] - K_{deg}^{p21}[p21] - K_{deg}^{p21,Pt}\frac{[Dam\_Pt]^3}{(J_{Pt}^{p21})^3 + [Dam\_Pt]^3}[p21] - K_{deg}^{p21,Dox}\frac{[Dam\_Dox]^3}{(J_{Dox}^{p21})^3 + [Dam\_Dox]^3}[p21] \quad \text{E17}$$

Modeling the cell viability response

To take into account cell viability response to cisplatin or doxorubicin treatment, we modeled the cell population size with the following cell birth and death model:

$$\frac{d[viableCells]}{dt} = K_{birth}^{CellType}[viableCells] - (H(Pt)K_{death}^{Pt} + H(Dox)K_{death}^{Dox})\,([p53s] - \theta)H([p53s] - \theta))[viableCells] \quad \text{E18}$$

$$[p53s] = [p53] + [p53pS15] \quad \text{E19}$$

$$Viability(t) = \frac{viableCells(t)}{e^{t \cdot K_{birth}^{CellType}}} \quad \text{E20}$$

The parameter $K_{birth}^{CellType}$ is characterized by the doubling time of each cell type ($K_{birth}^{CellType} = \frac{log(2)}{doubling\ time}$). The measured doubling time is about 64 hours and 42 hours for breast and lung cells, respectively. The function $Viability(t)$ quantifies the ratio of viable cell number at time *t* after cisplatin or doxorubicin treatment compared to the control sample under normal growth.

Previous studies have indicated that a threshold mechanism mediates p53 cell fate decision to induce apoptosis (Kracikova et al., 2013; Paek et al., 2016). In this work, we proposed a novel "friction model" to describe cell apoptosis response with a coarse-grained model, in which a hypothetical threshold mechanism is used for the trigger of apoptosis. We assume that the cells undergo apoptosis (cell death) when total p53 level is higher than a certain threshold, θ. Instead of using a fixed threshold, we assume that the threshold θ is proportional to the level of p21 expression because p21 has been reported as an important negative regulator for apoptosis (Abbas and Dutta, 2009; Roninson, 2002) and our data show p21 inhibition reduces viability. This dynamic threshold is analogous to the friction force exerted by a surface that resists the motion of an object. The friction force is proportional to the weight (mass) of the object. In order to move cells to apoptosis, the driving force (induced by p53) should be larger than the friction force (induced by p21). We modeled the threshold (θ) of p53 level for apoptosis with the following equation:

$$\theta = \mu[p21] \quad \text{E21}$$

Steady state analysis of the model before DNA damage stress stimulation

Before cisplatin or doxorubicin treatment, the model for the DNA damage response system is in steady state, at which $\frac{d[x_i]}{dt} = 0$ (x_i is a ODE variable in the differential equations), corresponding to a set of algebraic equations. By solving these algebraic equations, we obtained the following initial steady state solutions:

$$[Pt\_cell]_0^{ss} = 0 \quad \text{E22}$$

$$[DNA\_Pt]_0^{ss} = 0 \quad \text{E23}$$

$$[Dam\_Pt]_0^{ss} = 0 \quad \text{E24}$$

$$[Dox\_cell]_0^{ss} = 0 \quad \text{E25}$$

$$[Dam\_Dox]_0^{ss} = 0 \quad \text{E26}$$

$$[Chk1]_0^{ss} = \frac{K_{prd}^{Chk1}}{K_{deg}^{Chk1}} \quad \text{E27}$$

$$[Chk1pS345]_0^{ss} = 0 \quad \text{E28}$$

$$[Chk2]_0^{ss} = \frac{K_{prd,CellType}^{Chk2}(K_{deg,CellType}^{Chk2p} + K_{depho}^{Chk2})}{K_{deg}^{Chk2}K_{deg,CellType}^{Chk2p} + K_{deg}^{Chk2}K_{depho}^{Chk2} + K_{deg,CellType}^{Chk2p}K_{pho1,CellType}^{Chk2}} \quad \text{E29}$$

$$[Chk2pT68]_0^{ss} = \frac{K_{prd,CellType}^{Chk2}K_{pho1,CellType}^{Chk2}}{K_{deg}^{Chk2}K_{deg,CellType}^{Chk2p} + K_{deg}^{Chk2}K_{depho}^{Chk2} + K_{deg,CellType}^{Chk2p}K_{pho1,CellType}^{Chk2}} \quad \text{E30}$$

$$[NFR]_0^{ss} = \frac{K_{prd,CellType}^{NFR}}{K_{deg1}^{NFR} + K_{deg2}^{NFR}[Chk2pT68]_0^{ss}} \quad \text{E31}$$

$$[p53]_0^{ss} = \frac{K_{prd,CellType}^{p53}}{K_{deg1}^{p53} + K_{deg2}^{p53}[NFR]_0^{ss}} \quad \text{E32}$$

$$[p53pS15]_0^{ss} = 0 \quad \text{E33}$$

$$[p21]_0^{ss} = \frac{K_{prd1}^{p21} + K_{prd2,CellType}^{p21}[Chk2pT68]_0^{ss}}{K_{deg,CellType}^{p21}} \quad \text{E34}$$

$[viableCells]_0^{ss} = 1$, *viableCells* indicates the relative number of viable cells normalized to the initial cell number before DNA damage treatment E35

Initial conditions of the model

The initial conditions of the model have a relative concentration unit. We set the total level of Chk1, Chk2, p53 and p21 to be 1 for lung cells. Therefore, the concentrations for these proteins in breast cells represent their relative levels to the corresponding proteins in lung cells. We compared the relative amount of Chk1, Chk2, p53 and p21 proteins in breast and lung cells with quantitative immunoblotting experiments. Table S5 shows the ratios of protein abundance per cell in HMEpC breast cells compared to those in HSAEpC lung cells. The experimental data shows that both breast and lung cells have similar abundance of Chk1 and Chk2 proteins. In the model, we set $[Chk1]_0^{ss} = 1$ and $Chk2s = [Chk2]_0^{ss} + [Chk2pT68]_0^{ss} = 1$ for both breast and lung cells. As the basal levels of Chk1pS345 and p53pS15 are very low, we assumed that $[Chk1pS345]_0^{ss} = 0$ and $[p53pS15]_0^{ss} = 0$. The detailed initial concentrations of the model are listed in Table S6.

Parameter estimation

Parameter estimation was performed with a parallel parameter estimation tool SBML-PET-MPI (Zi, 2011). To optimize model parameters, we applied a global optimization algorithm using a stochastic ranking evolution strategy (Runarsson and Yao, 2000) to minimize the sum of squares of differences between model simulations and the corresponding experimental datasets. The average values of experimental data were used for parameter estimation. The model was calibrated with time course and dose response data for most of the signaling molecules mentioned in the model. During parameter estimation, the model simulations have been simultaneously fit to about 192 average data points based on 976 experimental measurements from HMEpC breast and HSAEpC lung cells with cisplatin or doxorubicin treatment. In the model optimization process, we evaluated millions of parameter sets by running the parameter estimation tool on a computer cluster until a stable optimum was reached. The values of model parameters are listed in Table S7.

The detailed comparison of model simulations and corresponding experimental data sets are presented in Figure 3-5 and Figure S8, S14, S18. Overall, the model is able to quantitatively reproduce the dynamics of DNA-bound cisplatin (*Pt_DNA*), intracellular doxorubicin (*Dox_cell*), *Chk1*, *Chk1pS345*, *Chk2*, *Chk2pT68*, *p53*, *p53pS15*, *p21* and cell viability data in both HMEpC and HSAEpC cells with cisplatin or doxorubicin treatment. Model simulations are qualitatively consistent with experimental data sets when Chk1 and Chk2 inhibitors are added (Figure 4, S15).

Model predictions for the inhibition of Chk1 and Chk2 activities

To study the role of Chk1 and Chk2 activities in the regulation of downstream p53 and p21 responses, we performed model predictions for the inhibition of Chk1 and Chk2 activities. To simulate the effect of inhibiting Chk1 and Chk2 activity, we modified the ODEs for the following affected proteins:

$$\frac{d[p53]}{dt} = K_{prd}^{p53} - K_{deg1}^{p53}[p53] - K_{deg2}^{p53}[NFR][p53] + K_{depho}^{p53}[p53pS15] - \left(\frac{K_{pho1}^{p53}\left([Chk1pS345](1-Chk1i)\right)^3}{(J_1^{p53})^3 + \left([Chk1pS345](1-Chk1i)\right)^3} + \frac{K_{pho2}^{p53}([Chk2pT68](1-Chk2i))^3}{(J_2^{p53})^3 + ([Chk2pT68](1-Chk2i))^3}\right) \quad \text{E36}$$

$$\frac{d[p53pS15]}{dt} = + \left(\frac{K_{pho1}^{p53}\left([Chk1pS345](1-Chk1i)\right)^3}{(J_1^{p53})^3 + \left([Chk1pS345](1-Chk1i)\right)^3} + \frac{K_{pho2}^{p53}\left([Chk2pT68](1-Chk2i)\right)^3}{(J_2^{p53})^3 + \left([Chk2pT68](1-Chk2i)\right)^3}\right) - K_{deg1}^{p53p}[p53pS15] - K_{deg2}^{p53p}[NFR][p53pS15] - K_{depho}^{p53}[p53pS15] \quad \text{E37}$$

$$\frac{d[NFR]}{dt} = K_{prd1}^{NFR} + K_{prd2}^{NFR}\frac{[z2]^3}{(J_{p53p}^{NFR})^3 + [z2]^3} - K_{deg1}^{NFR}[NFR] - K_{deg2}^{NFR}[Chk1pS345](1-Chk1i) - K_{deg3}^{NFR}[Chk2pT68](1-Chk2i)) \quad \text{E38}$$

$$\frac{d[p21]}{dt} = K_{prd1}^{p21} - K_{deg}^{p21}[p21] + \left(K_{prd2,CellType}^{p21} + (H(Pt)K_{prd3}^{p21,Pt} + H(Dox)K_{prd3}^{p21,Dox})\frac{[z2]^3}{(J_{p53p}^{p21})^3 + [z2]^3}\right)[Chk2pT68](1-Chk2i) \quad \text{E39}$$

$$-K_{deg}^{p21,Pt}\frac{[Dam\_Pt]^3}{\left(J_{Pt}^{p21}\right)^3+[Dam\_Pt]^3}[p21]-K_{deg}^{p21,Dox}\frac{[Dam\_Dox]^3}{\left(J_{Dox}^{p21}\right)^3+[Dam\_Dox]^3}[p21]$$

where *z2* represents for $p53pS15(t-\tau)$

$Chk1i = 0$, for no inhibition of $Chk1$ activity;
$Chk1i = 0.9$, for simulation with 90% inhibition of $Chk1$ activity; E40

$Chk2i = 0$, for no inhibition of $Chk2$ activity ;
$Chk2i = 0.9$, for simulation with 90% inhibition of $Chk2$ activity; E41

Supplemental References

Abbas, T., and Dutta, A. (2009). p21 in cancer: intricate networks and multiple activities. Nat Rev Cancer *9*, 400-414.

Aliouat-Denis, C.M., Dendouga, N., Van den Wyngaert, I., Goehlmann, H., Steller, U., van de Weyer, I., Van Slycken, N., Andries, L., Kass, S., Luyten, W.*, et al.* (2005). p53-independent regulation of p21Waf1/Cip1 expression and senescence by Chk2. Mol Cancer Res *3*, 627-634.

Barr, A.R., Cooper, S., Heldt, F.S., Butera, F., Stoy, H., Mansfeld, J., Novak, B., and Bakal, C. (2017). DNA damage during S-phase mediates the proliferation-quiescence decision in the subsequent G1 via p21 expression. Nat Commun *8*, 14728.

Batchelor, E., Loewer, A., Mock, C., and Lahav, G. (2011). Stimulus-dependent dynamics of p53 in single cells. Mol Syst Biol *7*, 488.

Batchelor, E., Mock, C.S., Bhan, I., Loewer, A., and Lahav, G. (2008). Recurrent initiation: a mechanism for triggering p53 pulses in response to DNA damage. Mol Cell *30*, 277-289.

Bloom, J., Amador, V., Bartolini, F., DeMartino, G., and Pagano, M. (2003). Proteasome-mediated degradation of p21 via N-terminal ubiquitinylation. Cell *115*, 71-82.

Bohgaki, M., Hakem, A., Halaby, M.J., Bohgaki, T., Li, Q., Bissey, P.A., Shloush, J., Kislinger, T., Sanchez, O., Sheng, Y.*, et al.* (2013). The E3 ligase PIRH2 polyubiquitylates CHK2 and regulates its turnover. Cell Death Differ *20*, 812-822.

Burger, H., Zoumaro-Djayoon, A., Boersma, A.W., Helleman, J., Berns, E.M., Mathijssen, R.H., Loos, W.J., and Wiemer, E.A. (2010). Differential transport of platinum compounds by the human organic cation transporter hOCT2 (hSLC22A2). Br J Pharmacol *159*, 898-908.

Centerwall, C.R., Tacka, K.A., Kerwood, D.J., Goodisman, J., Toms, B.B., Dubowy, R.L., and Dabrowiak, J.C. (2006). Modification and uptake of a cisplatin carbonato complex by Jurkat cells. Mol Pharmacol *70*, 348-355.

Chen, L., Gilkes, D.M., Pan, Y., Lane, W.S., and Chen, J. (2005). ATM and Chk2-dependent phosphorylation of MDMX contribute to p53 activation after DNA damage. EMBO J *24*, 3411-3422.

Dennis, G., Jr., Sherman, B.T., Hosack, D.A., Yang, J., Gao, W., Lane, H.C., and Lempicki, R.A. (2003). DAVID: Database for Annotation, Visualization, and Integrated Discovery. Genome Biol *4*, P3.

Dimri, G., Band, H., and Band, V. (2005). Mammary epithelial cell transformation: insights from cell culture and mouse models. Breast Cancer Res *7*, 171-179.

El-Kareh, A.W., and Secomb, T.W. (2003). A mathematical model for cisplatin cellular pharmacodynamics. Neoplasia *5*, 161-169.

El-Kareh, A.W., and Secomb, T.W. (2005). Two-mechanism peak concentration model for cellular pharmacodynamics of Doxorubicin. Neoplasia *7*, 705-713.

Garcia-Limones, C., Lara-Chica, M., Jimenez-Jimenez, C., Perez, M., Moreno, P., Munoz, E., and Calzado, M.A. (2016). CHK2 stability is regulated by the E3 ubiquitin ligase SIAH2. Oncogene *35*, 4289-4301.

Huang da, W., Sherman, B.T., and Lempicki, R.A. (2009). Systematic and integrative analysis of large gene lists using DAVID bioinformatics resources. Nat Protoc *4*, 44-57.

Jin, Y., Dai, M.S., Lu, S.Z., Xu, Y., Luo, Z., Zhao, Y., and Lu, H. (2006). 14-3-3gamma binds to MDMX that is phosphorylated by UV-activated Chk1, resulting in p53 activation. EMBO J *25*, 1207-1218.

Jin, Y., Lee, H., Zeng, S.X., Dai, M.S., and Lu, H. (2003). MDM2 promotes p21waf1/cip1 proteasomal turnover independently of ubiquitylation. EMBO J *22*, 6365-6377.

Kass, E.M., Ahn, J., Tanaka, T., Freed-Pastor, W.A., Keezer, S., and Prives, C. (2007). Stability of checkpoint kinase 2 is regulated via phosphorylation at serine 456. J Biol Chem *282*, 30311-30321.

Kracikova, M., Akiri, G., George, A., Sachidanandam, R., and Aaronson, S.A. (2013). A threshold mechanism mediates p53 cell fate decision between growth arrest and apoptosis. Cell Death Differ *20*, 576-588.

LeBron, C., Chen, L., Gilkes, D.M., and Chen, J. (2006). Regulation of MDMX nuclear import and degradation by Chk2 and 14-3-3. EMBO J *25*, 1196-1206.

Loughery, J., Cox, M., Smith, L.M., and Meek, D.W. (2014). Critical role for p53-serine 15 phosphorylation in stimulating transactivation at p53-responsive promoters. Nucleic Acids Res *42*, 7666-7680.

Love, I.M., and Grossman, S.R. (2012). It Takes 15 to Tango: Making Sense of the Many Ubiquitin Ligases of p53. Genes Cancer *3*, 249-263.

Ma, L., Wagner, J., Rice, J.J., Hu, W., Levine, A.J., and Stolovitzky, G.A. (2005). A plausible model for the digital response of p53 to DNA damage. Proc Natl Acad Sci U S A *102*, 14266-14271.

Macleod, K.F., Sherry, N., Hannon, G., Beach, D., Tokino, T., Kinzler, K., Vogelstein, B., and Jacks, T. (1995). p53-dependent and independent expression of p21 during cell growth, differentiation, and DNA damage. Genes Dev *9*, 935-944.

Nagasawa, K., Natazuka, T., Chihara, K., Kitazawa, F., Tsumura, A., Takara, K., Nomiyama, M., Ohnishi, N., and Yokoyama, T. (1996). Transport mechanism of anthracycline derivatives in human leukemia cell lines: uptake and efflux of pirarubicin in HL60 and pirarubicin-resistant HL60 cells. Cancer Chemother Pharmacol *37*, 297-304.

Paek, A.L., Liu, J.C., Loewer, A., Forrester, W.C., and Lahav, G. (2016). Cell-to-Cell Variation in p53 Dynamics Leads to Fractional Killing. Cell *165*, 631-642.

Roninson, I.B. (2002). Oncogenic functions of tumour suppressor p21(Waf1/Cip1/Sdi1): association with cell senescence and tumour-promoting activities of stromal fibroblasts. Cancer Lett *179*, 1-14.

Runarsson, T.P., and Yao, X. (2000). Stochastic ranking for constrained evolutionary optimization. Ieee Transactions on Evolutionary Computation *4*, 284-294.

Stewart-Ornstein, J., and Lahav, G. (2017). p53 dynamics in response to DNA damage vary across cell lines and are shaped by efficiency of DNA repair and activity of the kinase ATM. Sci Signal *10*.

van Jaarsveld, M.T., Wouters, M.D., Boersma, A.W., Smid, M., van Ijcken, W.F., Mathijssen, R.H., Hoeijmakers, J.H., Martens, J.W., van Laere, S., Wiemer, E.A.*, et al.* (2014). DNA damage responsive microRNAs misexpressed in human cancer modulate therapy sensitivity. Mol Oncol *8*, 458-468.

Zhang, X.P., Liu, F., and Wang, W. (2011). Two-phase dynamics of p53 in the DNA damage response. Proc Natl Acad Sci U S A *108*, 8990-8995.

Zhang, Y.W., Brognard, J., Coughlin, C., You, Z., Dolled-Filhart, M., Aslanian, A., Manning, G., Abraham, R.T., and Hunter, T. (2009). The F box protein Fbx6 regulates Chk1 stability and cellular sensitivity to replication stress. Mol Cell *35*, 442-453.

Zhang, Y.W., Otterness, D.M., Chiang, G.G., Xie, W., Liu, Y.C., Mercurio, F., and Abraham, R.T. (2005). Genotoxic stress targets human Chk1 for degradation by the ubiquitin-proteasome pathway. Mol Cell *19*, 607-618.

Zi, Z. (2011). SBML-PET-MPI: a parallel parameter estimation tool for Systems Biology Markup Language based models. Bioinformatics *27*, 1028-1029.

Zi, Z., Zheng, Y., Rundell, A.E., and Klipp, E. (2008). SBML-SAT: a systems biology markup language (SBML) based sensitivity analysis tool. BMC Bioinformatics *9*, 342.